博士研究生国家奖学金申请审批表

<table>
<tr><td rowspan="6">基本情况</td><td>姓名</td><td>徐勇</td><td>性别</td><td>男</td><td>出生年月</td><td>1987.09</td></tr>
<tr><td>政治面貌</td><td>群众</td><td>民族</td><td>汉族</td><td>入学时间</td><td>2018.09</td></tr>
<tr><td>学院</td><td>理学院</td><td>专业</td><td>物理学</td><td>学号</td><td>11849470</td></tr>
<tr><td>学制</td><td>4 年</td><td>攻读学位</td><td>博士</td><td>学生类别</td><td>普通博士</td></tr>
<tr><td colspan="6">是否在 2021 年 9 月 30 日前完成开题且未完成预答辩：是 ☑　　　　否☐</td></tr>
<tr><td>身份证号</td><td colspan="5"></td></tr>
<tr><td>申请理由</td><td colspan="6">本人 2018 年秋季入学攻读博士学位，读博期间积极参与导师在拓扑材料量子输运领域的研究工作，并取得了系列研究成果，具体如下：
● 以第一或共一作者身份在物理学领域核心期刊发表 SCI 论文 3 篇，分别为 Physical Review Letters (IF=9.161, Q1，第一作者) 、 Applied Physics Letters (IF=3.791, Q2，第一作者)和 Journal of Applied Physics (IF=2.646, Q2，共同一作)。其中第 1 篇报道了利用拓扑材料表面态的量子隧穿效应设计出了一种不需要拓扑相变的高效拓扑场效应管；第 2 篇文章在此基础上研究了拓扑场效应管在磁场下的输运性质，获得了开关比高达 10^{10} 的巨磁阻效应；第 3 篇文章报道了硅烯在非均匀分布的应力作用下可以实现量子反常霍尔效应。
● 在项目参与方面，参与了 2 项导师的国家自然科学基金面上项目， 在项目“狄拉克材料中超导异质结的输运性质研究”（No.11774144）中主要承担关于石墨烯以及外尔半金属材料超导异质结的输运性质的理论数值计算；在项目“马约拉纳零能模输运信号的理论研究”（2021 年获批）中主要承担马约拉纳模的约瑟夫森效应的研究工作。
● 学术交流方面，2019 年 9 月参加了郑州大学承办的中国物理学会年会，加深理解了物理学特别是拓扑材料领域的研究现状。2020 年 12 月以志愿者身份参加了南方科技大学量子研究院举办的量子信息物理论坛，了解了一些前沿研究工作。2021 年 7 月，线上参加了河北师范大学举办的凝聚态理论暑期讲习班，学习一些新的物理知识和研究方法。
以上是我的申请理由，敬请各位评委老师审核、批准。

申请人签名：徐勇

2021 年　10 月　8　日</td></tr>
</table>

<table>
<tr><td>推荐
意见</td><td colspan="2">徐勇同学学习思想端正，认真努力，积极参与课题组相关领域的研究工作，取得了一定学术成果，其中有 3 篇文章发表于物理学核心期刊上；同时该学生乐观开朗，积极参与集体活动，团队合作意识较强。综合各方面表现，推荐其申请国家奖学金。

推荐人（导师）签名：徐虎
2021 年 10 月 8 日</td></tr>
<tr><td>审核
意见</td><td>学生所在党支部意见：

（党支部填）
支部书记签名：
年 月 日</td><td>基层党委意见：

（学院党委填）
党委书记签名（公章）：
年 月 日</td></tr>
<tr><td>评审
情况</td><td colspan="2">经评审，并在本单位内公示____5____个工作日，无异议，推荐该同学获得研究生国家奖学金。
（学院评审主任委员签名，不需盖公章） 评审委员会主任委员签名：
年 月 日</td></tr>
<tr><td>基层单位意见</td><td colspan="2">经评审，并在本单位内公示____5____个工作日，无异议，本单位申报该同学获得研究生国家奖学金。现报请研究生国家奖学金评审领导小组审定。
基层单位主管领导签名：
（南科大研究生院填） （基层单位公章）
年 月 日</td></tr>
<tr><td>培养单位意见</td><td colspan="2">经审核，并在本单位公示______个工作日，无异议，现批准该同学获得研究生国家奖学金。

（哈工大填）

（培养单位公章）
年 月 日</td></tr>
</table>

学生操作手册（PDF）下载 学生 徐勇 ，欢迎您！ 退出

菜单 快捷

学籍服务
培养服务
- 培养计划申请
- 课程信息查看
- 培养方案查询
- 选教学班
- 课表查询
- 论文开题考核申请
- 论文开题考核修改
- 博士资格考试申请
- 语言类成绩录入
- 校外成绩录入
- 培养环节申请
- 成绩查询
- 重修申请
- 缓考申请
- 学生考场安排信息查看

奖助服务
成果录入

培养服务 成绩查询

我的成绩信息

红色的课程成绩在报表中不会打印!

课程类别	学期	学期绩点	课程编号	课程	课程归属	学分	考试成绩	绩点	是否及格	考试性质
专业课	2018 秋季	3.72	PHY5001	高等量子力学	校内	4	93	4	及格	期末考试
	2019 春季	3.43	PHY5002	固体理论	校内	4	79	3	及格	期末考试
	2019 春季	3.43	PHY5008	量子输运理论	校内	3	90	4	及格	期末考试
	2018 秋季	3.72	PHY5009	密度泛函方法与固体电子结构基础	校内	3	89	3.7	及格	期末考试
	2018 秋季	3.72	PHY5028	凝聚态物理讲坛	校内	3	B+	3	及格	期末考试
公共课	2018 秋季	3.72	GGC5003	科技论文检索与写作	校内	2	99	4	及格	期末考试
	2018 秋季	3.72	GGC5016	博士英语	校内	2	90	4	及格	期末考试
	2018 秋季	3.72	GGC5021	中国马克思主义与当代	校内	2	86	3.7	及格	期末考试

学分统计信息：(总学分：23.0,学位课学分：23.0,平均绩点：3.63)

Applied Physics Letters

Giant magnetoresistance effect due to the tunneling between quantum anomalous Hall edge states

Cite as: Appl. Phys. Lett. **118**, 222401 (2021); https://doi.org/10.1063/5.0050224
Submitted: 12 March 2021 . Accepted: 14 May 2021 . Published Online: 01 June 2021

Yong Xu, Jun Wang, Jun-Feng Liu, and Hu Xu

AIP Publishing

Giant magnetoresistance effect due to the tunneling between quantum anomalous Hall edge states

Cite as: Appl. Phys. Lett. **118**, 222401 (2021); doi: 10.1063/5.0050224
Submitted: 12 March 2021 · Accepted: 14 May 2021 ·
Published Online: 1 June 2021

View Online Export Citation CrossMark

Yong Xu,[1,2,3] Jun Wang,[4] Jun-Feng Liu,[2,a] and Hu Xu[3,a]

AFFILIATIONS

[1]Department of Physics, Harbin Institute of Technology, Harbin 150001, China
[2]School of Physics and Materials Science, Guangzhou University, Guangzhou 510006, China
[3]Department of Physics, Southern University of Science and Technology, Shenzhen 518055, China
[4]Department of Physics, Southeast University, Nanjing 210096, China

[a]Authors to whom correspondence should to addressed: phjfliu@gzhu.edu.cn and xuh@sustech.edu.cn

ABSTRACT

A recent work predicted the tunneling effect between topological edge states where the tunneling probability is tuned by a transverse electric field [Xu *et al.*, Phys. Rev. Lett. **123**, 206801 (2019)]. Here we study this tunneling effect between quantum anomalous Hall edge states under a perpendicular magnetic field. It is shown that the tunneling probability depends exponentially on the magnetic field. We propose a magnetic transistor based on a quantum anomalous Hall ribbon to observe this effect experimentally. Numerical simulations show that the conductance of the device is very sensitive to the strength and direction of the magnetic field. The positive/negative magnetic field results in the on/off state of the transistor. A giant magnetoresistance is found, and the on/off ratio reaches up to greater than 10^{10} for a long ribbon. These findings should be useful for potential applications in magnetic read heads and magnetic field sensors.

Two-dimensional topological insulators (2DTIs), including quantum spin Hall insulators and quantum anomalous Hall insulators, have attracted great research interest for the potential applications in nanoelectronics.[1–7] 2DTIs not only provide dissipationless transport channels for the benefit of robustness against impurity scattering, but also are used to design topological transistors[8–14] in device applications. In such topological transistors, the on/off switch is usually realized by the topological phase transition which has been suggested to be controlled by an electric field,[9–15] a magnetic field,[15–17] a strain,[18] or even the pressure and temperature.[19,20] However, the experimental realization of the electric manipulation of topological transitions is still a challenge. A recent work proposed a topological transistor without topological transition based on the tunneling between quantum spin Hall edge states.[4] And the key element for achieving a high on/off ratio in such transistors[4,5] is two quite long ballistic edge state channels. This is still experimentally challenging in quantum spin Hall insulators because the spin-flip backscattering seems inevitable in a quite long helical quantum spin Hall edge channel,[21–29] whereas the situation is different for the quantum anomalous Hall (QAH) insulators which have been theoretically predicted[30–32] and experimentally realized in magnetically doped topological insulator thin films.[33] QAH insulators host chiral edge states and can prohibit the backscattering at a single edge because of the absence of backward state.[34] Therefore, the transistor based on QAH edge states should be more feasible in experiments.

On the other hand, in proposed transverse tunneling transistors, the tunneling probability and the conductance are tuned by a transverse electric field. However, the magnetic control of the tunneling probability has not been studied. In proposed transistors, the tunneling probability between two edge states depends sensitively on the energy gap induced by the so-called finite-size effect.[35] This gap stems from the overlap of two edge states at opposite edges and is very sensitive to the external magnetic field.[35] Therefore, a giant magnetoresistance (GMR) effect[36–46] can be expected in the tunneling transistor based on QAH insulators. It implies potential applications in data storage technologies.

In this Letter, we propose a magnetic transistor based on a QAH insulator ribbon and numerically calculate the GMR. The conductance of the device is very sensitive to the strength and direction of the magnetic field. For the positive (negative) magnetic field, the device is in the on (off) state due to the absence (presence) of the transversal tunneling process of electrons. The conductance and the on/off ratio are also sensitive to the length of the ribbon. For a long ribbon, the on/off ratio reaches up to greater than 10^{10}. These results may have potential applications in magnetic read heads and magnetic field sensors.

We consider a two-terminal device shown in Fig. 1(a). It is made of a QAH ribbon which contains a scattering region with a linearly increasing electric potential and an external magnetic field. The length and width of the central scattering region are L and W, respectively. A linearly distributed potential energy $U(x)$ in the range $[0, U]$ along the x direction is applied to the device as shown in Fig. 1(b). There also exists a perpendicular magnetic field along the z direction in the scattering region. The tight-binding Hamiltonian of the QAH insulator is given by[30]

$$H_{TI} = \sum_{\mathbf{r}} \Phi_{\mathbf{r}}^{\dagger} H_{\mathbf{r},\mathbf{r}} \Phi_{\mathbf{r}} + \sum_{\mathbf{r},\mathbf{r}_0} (\Phi_{\mathbf{r}}^{\dagger} H_{\mathbf{r},\mathbf{r}+\mathbf{r}_0} \Phi_{\mathbf{r}+\mathbf{r}_0} + \text{H.c.}), \quad (1)$$

where $\mathbf{r} = (x, y)$ is the site index, $\mathbf{r}_0 = \mathbf{x}$ or $\mathbf{y}$ represents the unit vectors along x or y direction, $\Phi_{\mathbf{r}} = (c_{\uparrow\mathbf{r}}, c_{\downarrow\mathbf{r}})^T$ is the field operator, and $c_{\uparrow\mathbf{r}}, c_{\downarrow\mathbf{r}}$ are annihilation operators of electrons at site $\mathbf{r}$ with spin $\uparrow$ and $\downarrow$, respectively. The components included in the Hamiltonian are

$$\begin{aligned} H_{\mathbf{r},\mathbf{r}} &= \left[C_0 - 4C_2/a^2 + U(\mathbf{r})\right]\sigma_0 + (M_0 - 4M_2/a^2)\sigma_z, \\ H_{\mathbf{r},\mathbf{r}+\mathbf{x}} &= (C_2/a^2)\sigma_0 + (M_2/a^2)\sigma_z - (iA_0/2a)\sigma_x, \\ H_{\mathbf{r},\mathbf{r}+\mathbf{y}} &= (C_2/a^2)\sigma_0 + (M_2/a^2)\sigma_z + (iA_0/2a)\sigma_y, \end{aligned} \quad (2)$$

where σ_0 and $\sigma_{x,y,z}$ are the 2×2 unit matrix and the Pauli matrices for spin. The parameters are $A_0 = 364.5$ meV nm, $M_2 = -686$ meV nm^2, $C_0 = 0$, $C_2 = -512$ meV nm^2, $M_0 = -10$ meV, and the lattice constant $a = 5$ nm. $U(\mathbf{r}) = U(x) = Ux/L$ describes a linear potential along the x direction in the scattering region $[0, L]$. We consider a perpendicular magnetic field along the z direction, $\mathbf{B} = (0, 0, B)$. By using the Landau gauge $\mathbf{A} = (-By, 0, 0)$, an extra phase, the magnetic Peierls phase is introduced to the hopping matrix elements as $\phi_{\mathbf{r},\mathbf{r}+\mathbf{r}_0} = (2\pi/\phi_0)\int_{\mathbf{r}}^{\mathbf{r}+\mathbf{r}_0} \mathbf{A}d\mathbf{l}$ with $\phi_0 = h/e$ being the magnetic flux quantum.

First, we discuss the influence of the magnetic field on the finite-size effect induced gap. We consider a long uniform QAH ribbon without the linear potential $U(x)$ and under a magnetic field $\mathbf{B}$. In this case, the wave vector along the x direction k_x is still a good quantum number. By diagonalizing the Hamiltonian, we can obtain the band structure of the QAH ribbon. The band structure with and without the applied magnetic field is shown in Fig. 2(a). In the absence of a magnetic field, two QAH edge states residing in the bulk gap are coupling due to the finite size of the ribbon in the y direction and open a small gap located at $k_x = 0$ and near $E = 7.48$ meV. When a negative magnetic field is applied, the position of the finite-size gap moves upward to higher energy, nearly at $E = 8.55$ meV. More importantly, the size of the gap increases, which implies that the negative magnetic field enhanced the coupling and the tunneling probability between two edge states. Conversely, for a positive magnetic field, the gap moves downward to lower energy and becomes smaller. It implies that the magnetic field along the z direction suppresses the coupling and the tunneling probability between two edge states. The increase (decrease) in the gap size as the function of the strength of a negative (positive) magnetic field is depicted in Fig. 2(b). For a weak magnetic field, the gap size increases or decreases nearly linearly with increasing magnetic field strength.

Next, we study the magnetic control of the conductance in the transistor shown in Fig. 1(a). We consider an incident electron injected from the left lead. The Fermi energy is chosen to reside in the bulk gap, but far away from the small gap induced by the edge state coupling. The electron will travel rightward via the edge state along the top edge and then enter the scattering region. In the scattering region, the small finite-size gap is modulated by the magnetic field as discussed above. On the other hand, a linear potential $U(x)$ is applied in the scattering region to shift the small gap to the Fermi energy at some position along the ribbon. This position is the so-called tunneling point (as shown in Fig. 1) where the tunneling process occurs.[4] When the tunneling occurs, the electron crosses the insulating bulk and is reflected into the leftward edge state at the bottom edge. For a long enough scattering region which contains the tunneling point (with suitable U), the tunneling probability is very close to 1, and thus, the conductance is zero. While for a fixed length of the scattering region,

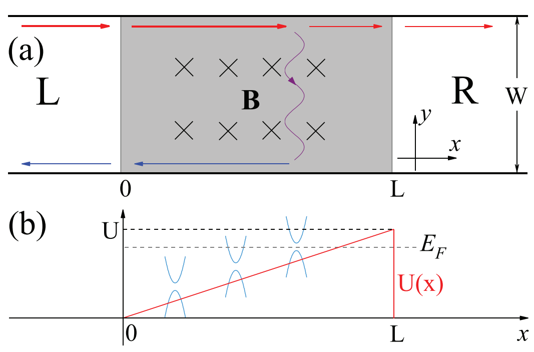

FIG. 1. (a) Schematic diagram of the magnetic transistor based on a QAH ribbon with two leads. The length and width of the scattering region are L and W, respectively. A perpendicular magnetic field **B** and a linear potential $U(x)$ are applied in the scattering region. (b) Profile of the linearly distributed potential energy $U(x)$ along the x direction.

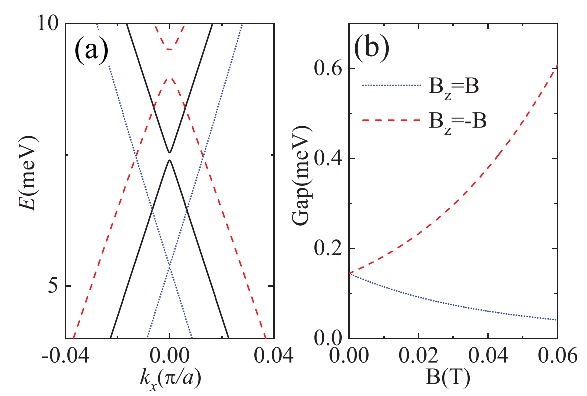

FIG. 2. (a) The band structure of the QAH ribbon without the magnetic field (black solid line), and with the positive (blue dot line) and negative (red dash line) magnetic field along the z direction. The width of the ribbon is $W = 50a$. The magnetic field strength is $B = 0.053T$. (b) The finite-size gaps due to the coupling between QAH edge states as functions of the strength of the magnetic field which is along $+z$ direction (blue dot line) and $-z$ direction (red dash line). The width $W = 50a$.

the tunneling probability depends exponentially on the small gap which is controlled by the magnetic field.

Therefore, it is expected that the conductance will depend exponentially on the magnetic field. We can define an on/off ratio R of the conductance for positive/negative magnetic fields,

$$R = \frac{G_B}{G_{-B}}. \tag{3}$$

Here, the two terminal conductances of the device G_B and G_{-B} are calculated by the lattice Green's function method in the Landauer–Büttiker formalism as follows:

$$G_B = \frac{e^2}{h} Tr[\Gamma_R G^r \Gamma_L G^a], \tag{4}$$

where $-e$ is the electron charge, h is the Planck's constant, and

$$G^r = \frac{1}{E - H_D - \Sigma_L^r - \Sigma_R^r}, \tag{5}$$

is the retarded Green's function, $G^a = [G^r]^\dagger$ is the advanced Green's function. H_D is the Hamiltonian of the scattering region. The linewidth function,

$$\Gamma_{R(L)} = i\left[\Sigma^r_{R(L)} - \Sigma^a_{R(L)}\right], \tag{6}$$

describes the coupling between the central device with the right (left) lead. $\Sigma^{r(a)}_{R(L)}$ is the retarded (advanced) self-energy for the right (left) lead calculated numerically by the recursive method.

Figure 3 shows the conductances of the device for positive and negative magnetic fields, and the on/off ratio, as functions of the magnetic field strength and the length of the scattering region. With increasing magnetic field strength, the positive magnetic field shrinks the small gap and enhances the conductance, while the negative magnetic field enhances the small gap and decreases the conductance exponentially, as shown in Fig. 3(a). Therefore, the on/off ratio of the conductance for positive/negative magnetic fields increases exponentially with increasing strength of the magnetic field as shown in Fig. 3(b). The width and length of the device are $W = 50a$ and $L = 5 \times 10^4 a$. An on/off ratio near 10^{10} is obtained by applied a weak magnetic field $B = 0.05T$. Note that the Onsager reciprocity relation is violated because the time reversal symmetry has been broken even in the absence of magnetic field. The generalized Onsager reciprocity relation will be $G_{12}(M_0, M_2, B) = G_{21}(-M_0, -M_2, -B)$, which has been verified by our numerical calculations.

Similarly, the conductance and the on/off ratio are also very sensitive to the length of the device. With the same strength of the magnetic field $0.053T$, the positive (negative) magnetic field induces a tiny (big) gap, as shown in Fig. 2(a). It is well known that the transmission probability and thus the conductance decays exponentially with the transport length of the evanescent wave. For the positive magnetic field, the conductance decreases approximately linearly with increasing length L as shown in Fig. 3(c). It is because that the gap is too tiny to exhibit the exponential decreasing. While for the negative magnetic field, the gap is big. We can clearly see that the conductance decreases exponentially with the length. Hence, as shown in Fig. 3(d), the on/off ratio exhibits well exponential increasing as the function of the length.

Finally, we confirm the robustness of the giant on/off ratio against impurities or disorders. We consider only nonmagnetic impurities. The situation is similar for magnetic impurities because the QAH edge states are robust against both nonmagnetic and magnetic impurities. The nonmagnetic impurities considered in the central scattering region are modeled by the random on-site potential $H_{dis} = \sum_{r,\uparrow(\downarrow)} D_r c^\dagger_{\uparrow(\downarrow)\mathbf{r}}(\sigma_0) c_{\uparrow(\downarrow)\mathbf{r}}$, where D_r is the random potential uniformly distributed in the interval $[-D_{dis}/2, D_{dis}/2]$ with D_{dis} the disorder strength. The averaged result of 100 samples is shown in Fig. 4 with the disorder strength $D_r = 10$ meV. Comparing with Figs. 3(c) and 3(d), the conductance for the negative magnetic field remains close to zero when $L > 2.5 \times 10^4 a$. And the conductance for the positive magnetic field exhibits only small fluctuations around the value without disorders. Therefore, the on/off ratio exhibits robust

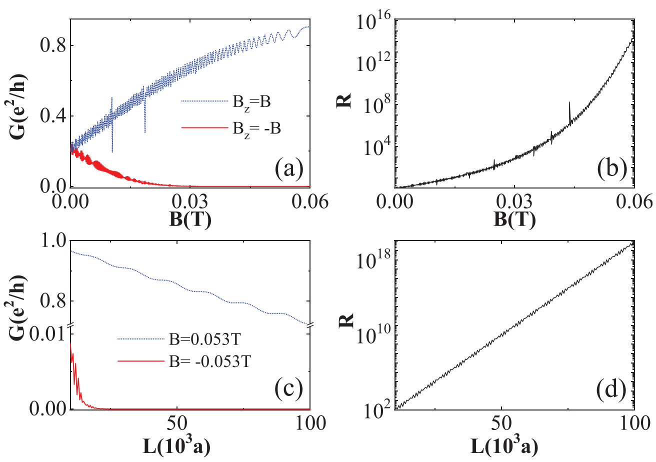

FIG. 3. (a) and (c) The conductance of the transistor vs the magnetic field strength B (a) and the length of the scattering region L (c), for the positive (blue dot line) and negative (red solid line) magnetic field, respectively. (b) and (d) The on/off ratio of the conductance vs the magnetic field strength B (b) and the length L (d). In (a) and (b), the length $L = 5 \times 10^4 a$. In (c) and (d), the magnetic field strength $B = 0.053T$. In (a)–(d), the Fermi energy is $E_F = 1$ meV, the minimum of the linear potential is $U = -11$ meV, and the width is $W = 50a$.

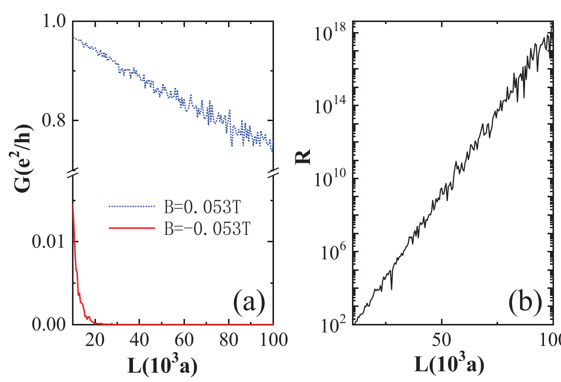

FIG. 4. The average conductances (a) and the average on/off ratio (b) of the 100 samples of the transistor with random nonmagnetic on-site disorders, as functions of the length L of the central scattering region. In (a), the blue dot (red solid) line is for the positive (negative) magnetic field. The other parameters are the same as those in Fig. 3.

exponential law with respect to the length L. Note that the disorder strength is 10 meV, much greater than the gap near 0.5 meV for the negative magnetic field.

In summary, we propose a magnetic transistor based on the tunneling between QAH edge states and study the influence of a perpendicular magnetic field on the conductance. The positive (negative) magnetic field decreases (increases) the finite-size gap due to the coupling between QAH edge states. The tunneling probability and hence the conductance depend exponentially on the gap. Therefore, the positive/negative magnetic field results in the on/off state of the transistor. A giant magnetoresistance is found, and the on/off ratio reaches up to greater than 10^{10} for a long ribbon. These findings should be useful for potential applications in magnetic read heads and magnetic field sensors.

The work described in this paper is supported by the National Natural Science Foundation of China (NSFC, Grant Nos. 11774144 and11874221).

DATA AVAILABILITY

The data that support the findings of this study are available from the corresponding authors upon reasonable request.

REFERENCES

[1]M. Konig, S. Wiedmann, C. Brune, A. Roth, H. Buhmann, L. W. Molenkamp, X.-L. Qi, and S.-C. Zhang, Science **318**, 766 (2007).
[2]M. Konig, H. Buhmann, L. W. Molenkamp, T. Hughes, C.-X. Liu, X.-L. Qi, and S.-C. Zhang, J. Phys. Soc. Jpn. **77**, 031007 (2008).
[3]A. Roth, C. Brune, H. Buhmann, L. W. Molenkamp, J. Maciejko, X.-L. Qi, and S.-C. Zhang, Science **325**, 294 (2009).
[4]Y. Xu, Y.-R. Chen, J. Wang, J.-F. Liu, and Z. Ma, Phys. Rev. Lett. **123**, 206801 (2019).
[5]H. Ishida and A. Liebsch, Phys. Rev. Res. **2**, 023242 (2020).
[6]J. Zheng, Y. Xiang, C. Li, R. Yuan, F. Chi, and Y. Guo, Phys. Rev. Appl. **14**, 034027 (2020).
[7]J.-E. Yang, X.-L. L, and H. Xie, New J. Phys. **22**, 103018 (2020).
[8]L. A. Wray, Nat. Phys. **8**, 705 (2012).
[9]M. Ezawa, Appl. Phys. Lett. **102**, 172103 (2013).
[10]J. Liu, T. H. Hsieh, P. Wei, W. Duan, J. Moodera, and L. Fu, Nat. Mater. **13**, 178 (2014).
[11]X. Qian, J. Liu, L. Fu, and J. Li, Science **346**, 1344 (2014).
[12]H. Pan, M. Wu, Y. Liu, and S. A. Yang, Sci. Rep. **5**, 14639 (2015).
[13]Q. Liu, X. Zhang, L. B. Abdalla, A. Fazzio, and A. Zunger, Nano Lett. **15**, 1222 (2015).
[14]Z. Zhang, X. Feng, J. Wang, B. Lian, J. Zhang, C. Chang, M. Guo, Y. Ou, Y. Feng, S.-C. Zhang, K. He, X. Ma, Q.-K. Xue, and Y. Wang, Nat. Nanotechnol. **12**, 953 (2017).
[15]A. Molle, J. Goldberger, M. Houssa, Y. Xu, S.-C. Zhang, and D. Akinwande, Nat. Mater. **16**, 163 (2017).
[16]A. M. Kadykov, F. Teppe, C. Consejo, L. Viti, M. S. Vitiello, S. S. Krishtopenko, S. Ruffenach, S. V. Morozov, M. Marcinkiewicz, W. Desrat, N. Dyakonova, W. Knap, V. I. Gavrilenko, N. N. Mikhailov, and S. A. Dvoretsky, Appl. Phys. Lett. **107**, 152101 (2015).
[17]M. Ezawa, Phys. Rev. Lett. **121**, 116801 (2018).
[18]S. Guan, Z.-M. Yu, Y. Liu, G.-B. Liu, L. Dong, Y. Lu, Y. Yao, and S. A. Yang, npj Quantum Mater. **2**, 23 (2017).
[19]S. S. Krishtopenko, I. Yahniuk, D. B. But, V. I. Gavrilenko, W. Knap, and F. Teppe, Phys. Rev. B **94**, 245402 (2016).
[20]A. M. Kadykov, S. S. Krishtopenko, B. Jouault, W. Desrat, W. Knap, S. Ruffenach, C. Consejo, J. Torres, S. V. Morozov, N. N. Mikhailov, S. A. Dvoretskii, and F. Teppe, Phys. Rev. Lett. **120**, 086401 (2018).
[21]C. Wu, B. A. Bernevig, and S.-C. Zhang, Phys. Rev. Lett. **96**, 106401 (2006).
[22]J. I. Váyrynen, M. Goldstein, Y. Gefen, and L. I. Glazman, Phys. Rev. B **90**, 115309 (2014).
[23]L. Du, I. Knez, G. Sullivan, and R.-R. Du, Phys. Rev. Lett. **114**, 096802 (2015).
[24]J. Wang, Y. Meir, and Y. Gefen, Phys. Rev. Lett. **118**, 046801 (2017).
[25]C.-H. Hsu, P. Stano, J. Klinovaja, and D. Loss, Phys. Rev. B **97**, 125432 (2018).
[26]A. A. Bagrov, F. Guinea, and M. I. Katsnelson, arXiv:1805.11700.
[27]J. I. Váyrynen, D. I. Pikulin, and J. Alicea, Phys. Rev. Lett. **121**, 106601 (2018).
[28]P. Novelli, F. Taddei, A. K. Geim, and M. Polini, Phys. Rev. Lett. **122**, 016601 (2019).
[29]L. Lunczer, P. Leubner, M. Endres, V. L. Müller, C. Br üne, H. Buhmann, and L. W. Molenkamp, Phys. Rev. Lett. **123**, 047701 (2019).
[30]C.-X. Liu, X.-L. Qi, X. Dai, Z. Fang, and S.-C. Zhang, Phys. Rev. Lett. **101**, 146802 (2008).
[31]R. Yu, W. Zhang, H.-J. Zhang, S.-C. Zhang, X. Dai, and Z. Fang, Science **329**, 61 (2010).
[32]T.-B. Lan, Y. Xu, H. Tan, J. Wang, and J.-F. Liu, J. Appl. Phys. **126**, 104303 (2019).
[33]C.-Z. Chang, J. Zhang, X. Feng, J. Shen, Z. Zhang, M. Guo, K. Li, Y. Ou, P. Wei, L.-L. Wang, Z.-Q. Ji, Y. Feng, S. Ji, X. Chen, J. Jia, X. Dai, Z. Fang, S.-C. Zhang, K. He, Y. Wang, L. Lu, X.-C. Ma, and Q.-K. Xue, Science **340**, 167 (2013).
[34]C.-Z. Chang, W. Zhao, D. Y. Kim, P. Wei, J. K. Jain, C. Liu, M. H. W. Chan, and J. S. Moodera, Phys. Rev. Lett. **115**, 057206 (2015).
[35]B. Zhou, H.-Z. Lu, R.-L. Chu, S.-Q. Shen, and Q. Niu, Phys. Rev. Lett. **101**, 246807 (2008).
[36]M. N. Baibich, J. M. Broto, A. Fert, F. N. Van Dau, F. Petroff, P. Etienne, G. Creuzet, A. Friederich, and J. Chazelas, Phys. Rev. Lett. **61**, 2472 (1988).
[37]G. Binasch, P. Grnberg, F. Saurenbach, and W. Zinn, Phys. Rev. B **39**, 4828 (1989).
[38]C. H. Chen and W. J. Hsueh, Appl. Phys. Lett. **104**, 042405 (2014).
[39]S. Rachel and M. Ezawa, Phys. Rev. B **89**, 195303 (2014).
[40]F. R. Ahmad, Appl. Phys. Lett. **106**, 012109 (2015).
[41]H. Aireddy, S. Bhaumik, and A. K. Das, Appl. Phys. Lett. **107**, 232406 (2015).
[42]M. Zare, L. Majidi, and R. Asgari, Phys. Rev. B **95**, 115426 (2017).
[43]Y. Xu, S. Uddin, J. Wang, J. Wu, and J.-F. Liu, Sci. Rep. **7**, 7578 (2017).
[44]P. Tseng and W.-J. Hsueh, New J. Phys. **21**, 113035 (2019).
[45]F. Li, B. Yang, Y. Zhu, X. Han, and Y. Yan, Appl. Phys. Lett. **117**, 022412 (2020).
[46]H. Tan, Y. Xu, J. Wang, J.-F. Liu, and Z. Ma, J. Phys. D: Appl. Phys. **54**, 105303 (2021).

Quantized Field-Effect Tunneling between Topological Edge or Interface States

Yong Xu,[1,2] Yan-Ru Chen,[1,2] Jun Wang,[3] Jun-Feng Liu,[1,2,*] and Zhongshui Ma[4,5,†]

[1]*School of Physics and Electronic Engineering, Guangzhou University, Guangzhou 510006, China*
[2]*Department of Physics, Southern University of Science and Technology, Shenzhen 518055, China*
[3]*Department of Physics, Southeast University, Nanjing 210096, China*
[4]*School of Physics, Peking University, Beijing 100871, China*
[5]*Collaborative Innovation Center of Quantum Matter, Beijing 100871, China*

(Received 9 January 2019; revised manuscript received 8 September 2019; published 12 November 2019)

We study the tunneling through a two-dimensional topological insulator with topologically protected edge states. It is shown that the tunneling probability can be quantized in a broad parameter range, 0 or 1, tuned by an applied transverse electric field. Based on this field-effect tunneling, we propose two types of topological transistors based on helical edge or interface states of quantum spin Hall insulators separately. The quantized tunneling conductance is obtained and shown to be robust against nonmagnetic disorders. Usually, the topological transition is necessary in the operation of topological transistors. These findings provide a new strategy for the design of topological transistors without topological transitions.

DOI: 10.1103/PhysRevLett.123.206801

Introduction.—It is well known that the tunneling probability is usually very small and decays exponentially with the transport length in a normal insulator. One may wonder what the tunneling is like through a topological insulator (TI) in the presence of transverse surface or edge states. It is intuitively supposed that the coupling between two surface states at opposite surfaces is capable of an important role in the tunneling. It has been shown [1] that the coupling between the surface states at two opposite surfaces opens a gap in the surface states due to the so-called finite-size effect. The tunneling between Fermi-arc surface states through Weyl points is recently verified by the theoretical prediction [2] and the experimental observation of three-dimensional quantum Hall effect [3–5] in Weyl semimetals. The natural question is whether the perfect tunneling is possible between the edge or surface states at two opposite edges or surfaces in a gapped topological insulator.

In addition to providing dissipationless transport channels, TIs are also used to design topological transistors [6–12] in device applications for the benefit of robustness against impurity scattering. In such topological transistors, the off state is usually realized by opening a gap in the edge channels through a topological phase transition or the finite-size effect. The topological phase transitions have been suggested to be controlled by an electric field [7–13], a magnetic field [13–15], a strain [16], or even the pressure and temperature [17,18]. However, the experimental realization of the electric manipulation of topological transitions is still a challenge. Further, the gap opened by the finite-size effect is very small. It implies that the off state requires fine-tuning of the chemical potential and a very low temperature in longitudinal tunneling transistors along edge channels. Additionally, the nonlocal transistor based on the coupling of edge or surface states [19,20], the topological spin transistor based on spin [21–23], and the imperfect transistor based on the modulation of impurity scattering [24] have also been discussed.

In this Letter, we show that the tunneling between the edge or surface states at opposite boundaries can be perfect and tunable from 0 to 1 by an electric field. This transverse tunneling effect provides a new strategy for the design of topological transistors without topological transitions. We propose two types of transverse tunneling transistors based on helical edge and interface states of quantum spin Hall insulators separately and determine the conditions of quantized conductance for the on or off state, respectively. Compared with longitudinal tunneling transistors along edge channels, such transverse tunneling transistors overcome the challenge of fine-tuning of the chemical potential to reside in the small finite-size induced gap.

Tunneling between topological edge states.—We start by considering the tunneling between topological surface states. For simplicity, we consider a two-dimensional topological insulator (2DTI) such as HgTe/CdTe quantum wells [25–27]. When the Fermi energy lies inside the bulk gap, only the helical edge modes are responsible for the transport. In the absence of magnetic impurities, two sets of chiral edge states are degenerate for spin-up and spin-down electrons. Therefore, we consider only the tunneling between spin-down edge states. The physics is the same for spin-up edge states but with opposite chirality. In a 2DTI ribbon shown in Fig. 1(a), two chiral spin-down edge modes are coupled by the finite-size effect. The effective model used to describe the coupling can be written as

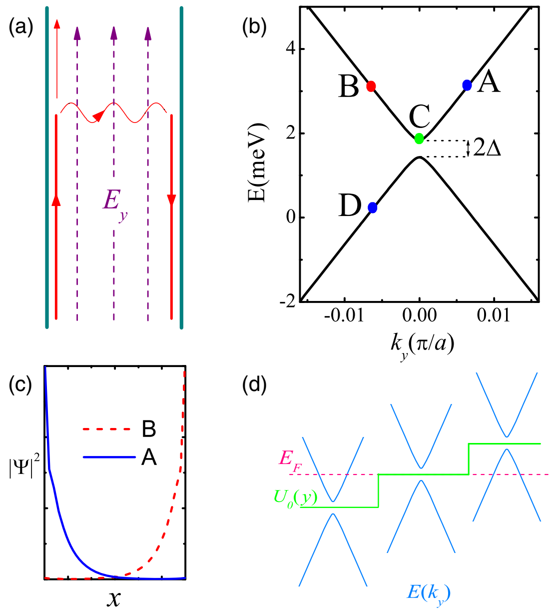

FIG. 1. (a) Sketch of the tunneling between topological edge states in a 2DTI under an electric field E_y. Only spin-down edge states are shown. (b) The band structure shows a gap due to the finite-size effect. (c) The wave function distributions of states A and B marked in (b). (d) The linear electrostatic potential U_y induced by the uniform electric field E_y can be simplified and modeled by two step functions.

$$H = \begin{pmatrix} \hbar v_F k & \Delta \\ \Delta & -\hbar v_F k \end{pmatrix}, \tag{1}$$

where $\pm\hbar v_F k$ denote the edge states at two edges and Δ describes the coupling between them. The finite-size induced gap Δ is related to the bulk gap Δ_0 by $\Delta = \Delta_0 e^{-2L/\xi}$ [28], where L is the width of the ribbon, and $\xi = \hbar v_F/\Delta_0$ is the penetration depth of the edge states. By solving the eigenproblem, we have eigenenergies $E_\pm = \pm\sqrt{\hbar^2 v_F^2 k^2 + \Delta^2}$ and corresponding eigenwave functions

$$\psi_\pm = \frac{1}{\sqrt{u^2 + \Delta^2}} \begin{pmatrix} \Delta \\ u \end{pmatrix} e^{iky} \tag{2}$$

with $u = E_\pm - \hbar v_F k$.

It is shown in Fig. 1(b) that the edge states are gapped by the finite-size effect. We consider the motion of an electron in the initial state A in the presence of an electric field E_y along the y direction. According to the equation of motion $\dot{k} = -eE_y/\hbar$, the electron will be slowed down by the electrostatic force and get to state C. Then the electron will either get to state B or cross the gap to get to state D. Figure 1(c) shows that states A and D locate at the left edge, while B locates at the right edge. If the electron evolves from state A to state B, it tunnels from the left edge to the right edge through the insulating bulk.

Beyond this semiclassical picture, we can also evaluate the probabilities of two processes by revisiting the evolution as a quantum scattering problem. The linear electrostatic potential induced by the uniform electric field can be simplified and modeled by two step functions, i.e., $U(y) = E[\Theta(y) + \Theta(y - w)]$, where E is the energy of the incident electron and $y \in [0, w]$ is the range in which the energy is inside the gap, as sketched in Fig. 1(d). We argue that this approximation is valid because the scattering will be possible only when the energy is around the gap. Far away from the gap, the coupling between the edge states at two sides will vanish and the scattering will be forbidden. For $y < 0$, the wave function is written as

$$\psi(y) = \begin{pmatrix} \Delta \\ u \end{pmatrix} e^{iky} + r \begin{pmatrix} u \\ \Delta \end{pmatrix} e^{-iky}, \tag{3}$$

where the wave vector $k = \sqrt{E^2 - \Delta^2}/(\hbar v_F)$ and $u = E - \hbar v_F k$. For simplicity, we consider only the situation of $E > 0$. In the area $y \in [0, w]$, the kinetic energy is zero and the wave function reads

$$\psi(y) = a \begin{pmatrix} 1 \\ -i \end{pmatrix} e^{-\Delta y/(\hbar v_F)} + b \begin{pmatrix} 1 \\ i \end{pmatrix} e^{\Delta y/(\hbar v_F)}. \tag{4}$$

For $y > w$, the wave function is

$$\psi(y) = t \begin{pmatrix} \Delta \\ -u \end{pmatrix} e^{-iky}. \tag{5}$$

By the continuity of the wave function at $y = 0$ and $y = w$, we can obtain the transverse transmission probability as follows:

$$T_y = |t|^2 = \frac{E^2 - \Delta^2}{E^2 \cosh^2[\Delta w/(\hbar v_F)]}. \tag{6}$$

Note that the tunneling probability along the x direction should be defined as $T_x = |r|^2 = 1 - T_y$. From Eq. (6), we can clearly see that the quantized tunneling will happen when $\Delta w/(\hbar v_F) \gg 1$. However, the tunneling probability will be very small when the electric field is absent. It formulates that the tunneling probability can be modulated by the transverse electric field.

Topological transistor based on edge state tunneling.— Based on this field-effect tunneling of edge states, we propose a topological transistor as shown in Fig. 2(a). In such an inverted T-shaped junction, a 2DTI quantum wire is connected with two metallic leads at the foot. The incident electron from the left lead first moves upward by means of the left edge state. Under the modulation of a transverse electric field, the electron may tunnel to the right side completely or do not tunnel at all. The conductance of the junction will be a conductance quantum for the former

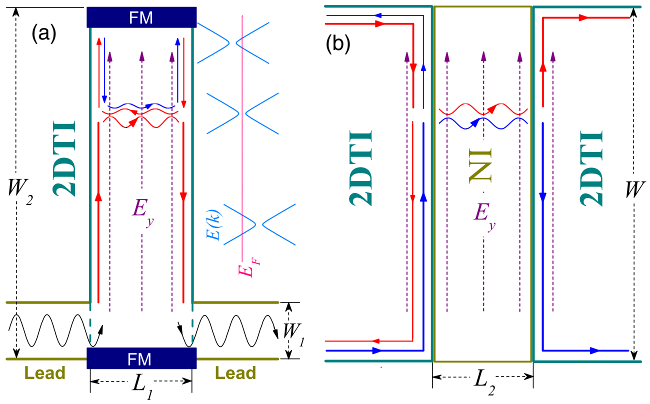

FIG. 2. Sketch of topological transistors based on (a) edge state and (b) interface state tunneling. In (a), a 2DTI quantum wire is connected with two metallic leads at the foot. Two ferromagnets (FMs) are deposited at the top and bottom of the wire to gap the edge channel. In (b), a normal insulator quantum wire are sandwiched between two 2DTI leads. The transverse electric field E_y is used to assist the tunneling between topological edge or interface states located at two edges or interfaces.

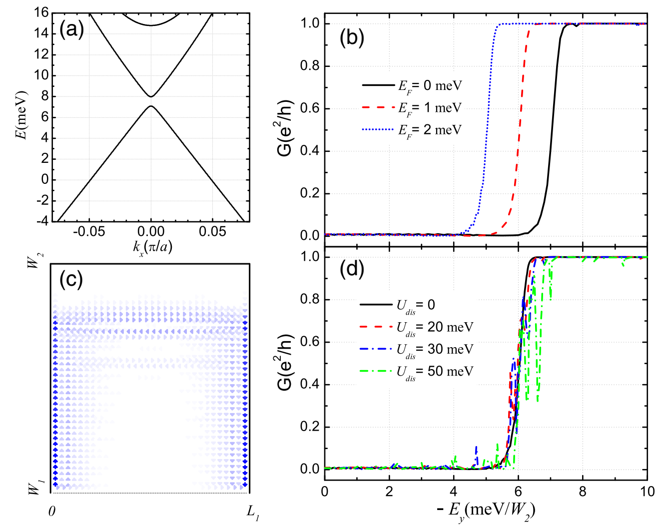

FIG. 3. Numerical results for the topological transistor based on edge state tunneling shown in Fig. 2(a). (a) Dispersion of edge states in a 2DTI quantum wire with the width $L_1 = 31a$. (b) Conductance as a function of the transverse electric field E_y for three chosen Fermi energies $E_F = 0$, 1, and 2 meV. Note that E_y is negative. (c) Current distribution for $E_F = 1$ meV and $E_y = 8$ meV. (d) Conductance in the presence of nonmagnetic disorders with various disorder strengths U_{dis} for $E_F = 1$ meV. Structure parameters are $W_1 = 30a$, $W_2 = 4000a$, and $L_1 = 31a$.

case, and zero for the latter case. To break the connectivity between the left and right edge states, two ferromagnets are deposited at the top and bottom of the wire to gap the edge channel.

We take HgTe/CdTe quantum wells as an example of the 2DTI. The effective Hamiltonian reads

$$H_{TI} = \epsilon(k) + \begin{pmatrix} M(k) & Ak_+ & 0 & 0 \\ Ak_- & -M(k) & 0 & 0 \\ 0 & 0 & M(k) & -Ak_- \\ 0 & 0 & -Ak_+ & -M(k) \end{pmatrix}, \quad (7)$$

where $\epsilon(k) = C - D(k_x^2 + k_y^2)$, $M(k) = M_0 - B(k_x^2 + k_y^2)$, and $k_\pm = k_x \pm ik_y$. In our calculation, the material parameters are taken as $A = 364.5$ meV nm, $B = -686$ meV nm^2, $C = 0$, $D = -512$ meV nm^2, and $M_0 = -10$ meV. The left and right leads are two normal quantum wires [29]. To calculate the conductance of such a junction, we first rewrite the tight-binding Hamiltonian of the junction in the square lattice. Then we calculate the conductance and current distribution by means of the lattice Green's function technique [29].

Figure 3 presents the numerical results of conductance and current distribution of an inverted T-shaped junction sketched in Fig. 2(a). The length of the 2DTI wire is $W_2 = 4000a$ (along the y direction) and the width is $L_1 = 31a$ (along the x direction, i.e., the transport direction), where a is the lattice constant. The width of the two leads is $W_1 = 30a$. The dispersion of edge states is shown in Fig. 3(a) where spin-up and spin-down edge states are degenerate. The finite-size effect induces the coupling between two edge states located at two edges and opens a small gap which is located near 7.5 meV. When incident electrons with the Fermi energy far below the gap (e.g., $E_F = 1$ meV) enter into the 2DTI from the left lead, only spin-down electrons can occupy the edge state to propagate upward along the edge. Without the electric field, spin-down electrons will be reflected to spin-up electrons by the top ferromagnet and then propagate downward, and finally go back to the left lead. In such a case, the conductance is zero. By applying a negative electric field, the potential can be decreased linearly along the 2DTI wire. If the electric field is big enough or the wire is long enough, there exists a region in the wire where the Fermi energy is located inside the gap. If the length of the region w is big enough, spin-down electrons will completely tunnel to the right edge according to Eq. (6). Now the conductance is a conductance quantum.

For a fixed finite-size-effect induced gap Δ, a big w means a weak electric field E_y due to $w = 2\Delta/E_y$. For a 2DTI ribbon with finite length W_2, the minimal potential difference between the bottom and the top should be $E_F - E_0$ to let the Fermi energy E_F cross the gap. Here E_0 denotes the energy of the center of gap. Therefore, the minimal electric field should be $(E_F - E_0)/W_2$. To make E_y small enough to get a quantized tunneling conductance, we need a big enough W_2. We consider a long 2DTI wire ($W_2 = 4000a$) to get a big w. The well-quantized conductances are obtained as functions of E_y for various E_F, as shown in Fig. 3(b). The electric field E_y causes a potential drop along the wire from bottom to top. For small E_y, the conductance is 0 because the tunneling does not occur. When E_y is big enough that the potential drop is larger than the difference between the gap position and E_F (7.5 meV–E_F), there exists a region in the wire where E_F is located inside the gap. Now the conductance becomes 1 due to the tunneling between edge states. The tunneling is verified by the current distribution sketched in Fig. 3(c). The main tunneling position is exactly within the region where E_F lies inside the gap. Figure 3(d) shows that the quantized conductance is also robust against nonmagnetic disorders which are modeled by the random on-site potential uniformly distributed in the interval $[-U_{\rm dis}/2, U_{\rm dis}/2]$ [29].

Topological transistor based on interface state tunneling.—We also propose a topological transistor based on interface state tunneling as shown in Fig. 2(b). A normal insulator (NI) quantum wire with the size $L_2 \times W$ are sandwiched between two 2DTI leads with the same width W. The incident electrons from the edge states of left 2DTI either go back to the left lead or tunnel to the right lead through the interface state tunneling between two interfaces. The well-quantized conductance is shown in Fig. 4. The parameters for 2DTI leads for the same with those in Fig. 3. The NI is also described by Eq. (7) but with only one different parameter $M_0 = 10$ meV. The turn-on electric field exactly corresponds to the potential increase from bottom to top which equals to the difference between E_F

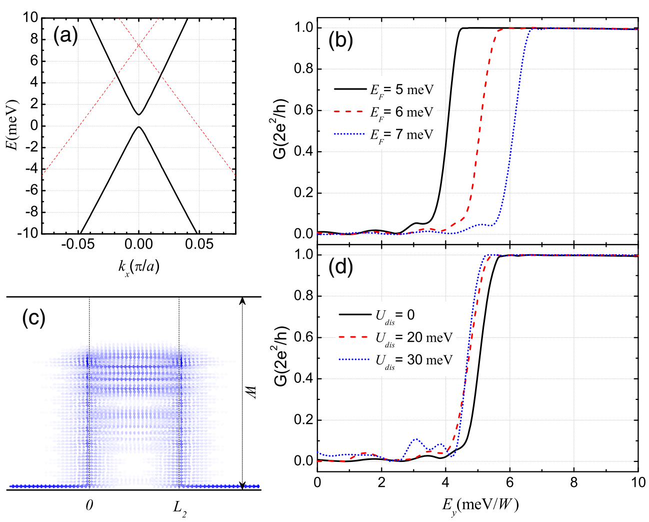

FIG. 4. Numerical results for the topological transistor based on interface state tunneling shown in Fig. 2(b). (a) Dispersion of a 2DTI/NI/2DTI quantum wire where a NI wire is sandwiched by two 2DTI wires. Solid black (dashed red) curves represent interface (edge) states. The width of the NI wire is $L_2 = 22a$. (b) Conductance as a function of E_y for three chosen Fermi energies $E_F = 5$, 6, and 7 meV. (c) Current distribution for $E_F = 6$ meV and $E_y = 7$ meV. Only spin-up electrons are considered. (d) Conductance in the presence of nonmagnetic disorders with various disorder strength $U_{\rm dis}$ for $E_F = 6$ meV. Structure parameters are $W = 4000a$ and $L_2 = 22a$.

and the gap [nearly $E_F - 0.5$ meV; see Figs. 4(a) and 4(b)]. The current distribution of spin-up electrons in Fig. 4(c) demonstrates the process of tunneling. The robustness of this tunneling effect is verified by the well-quantized conductance in the presence of nonmagnetic disorders, as shown in Fig. 4(d).

Quantization conditions.—We give a brief guide to obtain well-quantized conductance in such topological transistors. For the off state, even E_F is far away from the gap, and there still exists a low probability that the tunneling will occur. The low probability is found to be Δ^2/E_F^2 [29]. To obtain a sufficiently small conductance in the off state, we first choose a suitable width L_1 or L_2 of the central device wire which should be small enough to induce a sufficiently small Δ, according to $\Delta = \Delta_0 e^{-2L/\xi}$. Then we determine the length of the device wire W_2 or W, which should be large enough to satisfy the condition $\Delta w/(\hbar v_F) \gg 1$ according to Eq. (6), which ensures a well-quantized conductance of 1 or 2 in the on state.

Experimental feasibility.—Finally, we comment on the experimental feasibility of proposed topological transistors. To achieve a quantized tunneling, the edge or interface channel should be ballistic before the tunneling. For 2DTIs, it has been experimentally found that the backscattering nearly always induces a deviation from the quantized conductance for a long edge channel [25,27,30,31]. The possible underlying mechanisms have been extensively discussed, including the presence of an external magnetic field or magnetic impurities, an $e-e$ interaction through the third order perturbation [32–34], the coupling of edge modes to charge puddles [35,36], the edge reconstruction [37], and the effects of Rashba spin-orbit coupling [38,39], phonons [40], nuclear spins [41,42], disordered probes [43], coupling to external baths [44], noise [45], etc. A significant breakthrough was made very recently [46]. It was shown that the combined action of short-range nonmagnetic impurities located near the edges and on-site electron-electron interactions effectively creates noncollinear magnetic scatterers and, hence, results in strong backscattering, even at zero temperature. Experimentally, both the spatially resolved study of backscattering using scanning gate microscopy [47] and the Hall bar measurement [48] reported the ballistic transport and quantized conductance in samples with an edge channel length up to 2 μm. The edge length dependence of the resistance indicates that the coherence length is up to 4.4 μm [48].

The numerical calculations show that the edge channels with length $4000a$ will promise a quantized tunneling. For InAs/GaSb quantum wells, the lattice constance is approximately 0.6 nm. The length of ballistic channels $4000a = 2.4$ μm is quite promising in experiments, though still a little more than the 2 μm reported so far. Moveover, because of the small band gap in HgTe/CdHgTe and InAs/GaSb quantum wells, the experimental observation of well-quantized tunneling conductance should be performed at low temperature. The numerical calculations show that quantized tunneling conductance can persist at temperatures up to 10 K [29].

For a single edge, although the backscattering seems inevitable in a quite long quantum spin Hall edge channel, it is absent in a chiral edge channel because of the quantum anomalous Hall (QAH) effect. The reported ballistic channels in experiments are up to 2.4 mm in length [49]. Our proposed transistors can also work based on the tunneling between quantum anomalous Hall edge or interface states. For the transistor based on the QAH interface state tunneling, the setup is the same as that shown in Fig. 2(b). The results shown in Fig. 4 can also apply to QAH interface state tunneling, except with a change of the quantized conductance from 2 to 1. For the transistor based on the QAH edge state tunneling, we can propose a new longitudinal transistor which also possesses quantized conductances [29]. Therefore, the quantized tunneling effect should be also observable in transistors based on QAH insulators. It is worth noting that the search for QAH insulators at higher temperature, which in practice is smaller than the Curie temperature of ferromagnetism [50,51], is fast progressing [52,53].

More importantly, we note that a newly published work [54] reported the latest progress in the dissipationless transport of quantum spin Hall edge channels. Lunczer *et al.* successfully achieved quantized conductance even in long channels up to 13 μm in HgTe quantum well structures, through the flattening of the potential landscape by controlled gate training. With this technique, the use of quantized helical edge channel transport becomes feasible in macroscopic devices.

Conclusions.—In conclusion, we study in this Letter the tunneling between topological edge or interface states. It is found that the tunneling probability can be quantized and tunable by an electric field. We propose topological transistors based on edge or interface state tunneling in junctions including 2DTIs. The conductance can be quantized for a suitable size of the tunneling region and is also robust against nonmagnetic disorders. The proposed topological transistors are accessible in experiments and without topological transition in the operation. The finding sheds new light on the design of topological transistors.

The work described in this Letter is supported by the National Natural Science Foundation of China [(NSFC), Grants No. 11774144, No. 11774006, and No. 11574045], and the National Basic Research Program (NBRP) of China (Grant No. 2012CB921300).

*phjfliu@gzhu.edu.cn
†mazs@pku.edu.cn

[1] B. Zhou, H.-Z. Lu, R.-L. Chu, S.-Q. Shen, and Q. Niu, Phys. Rev. Lett. **101**, 246807 (2008).
[2] C. M. Wang, H.-P. Sun, H.-Z. Lu, and X. C. Xie, Phys. Rev. Lett. **119**, 136806 (2017).
[3] C. Zhang *et al.*, Nat. Commun. **8**, 1272 (2017).
[4] T. Schumann, L. Galletti, D. A. Kealhofer, H. Kim, M. Goyal, and S. Stemmer, Phys. Rev. Lett. **120**, 016801 (2018).
[5] C. Zhang *et al.*, Nature (London) **565**, 331 (2019).
[6] L. Andrew Wray, Nat. Phys. **8**, 705 (2012).
[7] M. Ezawa, Appl. Phys. Lett. **102**, 172103 (2013).
[8] J. Liu, T. H. Hsieh, P. Wei, W. Duan, J. Moodera, and L. Fu, Nat. Mater. **13**, 178 (2014).
[9] X. Qian, J. Liu, L. Fu, and J. Li, Science **346**, 1344 (2014).
[10] H. Pan, M. Wu, Y. Liu, and S. A. Yang, Sci. Rep. **5**, 14639 (2015).
[11] Q. Liu, X. Zhang, L. B. Abdalla, A. Fazzio, and A. Zunger, Nano Lett. **15**, 1222 (2015).
[12] Z. Zhang *et al.*, Nat. Nanotechnol. **12**, 953 (2017).
[13] A. Molle, J. Goldberger, M. Houssa, Y. Xu, S.-C. Zhang, and D. Akinwande, Nat. Mater. **16**, 163 (2017).
[14] A. M. Kadykov *et al.*, Appl. Phys. Lett. **107**, 152101 (2015).
[15] M. Ezawa, Phys. Rev. Lett. **121**, 116801 (2018).
[16] S. Guan, Z.-M. Yu, Y. Liu, G.-B. Liu, L. Dong, Y. Lu, Y. Yao, and S. A. Yang, npj Quantum Mater. **2**, 23 (2017).
[17] S. S. Krishtopenko, I. Yahniuk, D. B. But, V. I. Gavrilenko, W. Knap, and F. Teppe, Phys. Rev. B **94**, 245402 (2016).
[18] A. M. Kadykov, S. S. Krishtopenko, B. Jouault, W. Desrat, W. Knap, S. Ruffenach, C. Consejo, J. Torres, S. V. Morozov, N. N. Mikhailov, S. A. Dvoretskii, and F. Teppe, Phys. Rev. Lett. **120**, 086401 (2018).
[19] Z. Wang, J. Song, H. Liu, H. Jiang, and X. C. Xie, New J. Phys. **17**, 113040 (2015).
[20] Y. Xu, S. Uddin, J. Wang, J. Wu, and J.-F. Liu, Sci. Rep. **7**, 7578 (2017).
[21] V. Krueckl and K. Richter, Phys. Rev. Lett. **107**, 086803 (2011).
[22] J. Maciejko, E.-A. Kim, and X.-L. Qi, Phys. Rev. B **82**, 195409 (2010).
[23] F. Dolcini, Phys. Rev. B **83**, 165304 (2011).
[24] W. G. Vandenberghe and M. V. Fischetti, Nat. Commun. **8**, 14184 (2017).
[25] M. König, S. Wiedmann, C. Brüne, A. Roth, H. Buhmann, L. W. Molenkamp, X.-L. Qi, and S.-C. Zhang, Science **318**, 766 (2007).
[26] M. König, H. Buhmann, L. W. Molenkamp, T. L. Hughes, C.-X. Liu, X.-L. Qi, and S.-C. Zhang, J. Phys. Soc. Jpn. **77**, 031007 (2008).
[27] A. Roth, C. Brüne, H. Buhmann, L. W. Molenkamp, J. Maciejko, X.-L. Qi, and S.-C. Zhang, Science **325**, 294 (2009).
[28] M. Ezawa and N. Nagaosa, Phys. Rev. B **88**, 121401(R) (2013).
[29] See Supplemental Material at http://link.aps.org/supplemental/10.1103/PhysRevLett.123.206801 for the lattice Hamiltonians of two proposed topological transistors, the numerical methods to calculate the conductance and current distribution, the estimation of the tunneling probability in the off state, the transistor based on quantum anomalous Hall edge states, and the temperature dependence of tunneling conductance.

[30] K. Suzuki, Y. Harada, K. Onomitsu, and K. Muraki, Phys. Rev. B **87**, 235311 (2013).
[31] G. Grabecki *et al.*, Phys. Rev. B **88**, 165309 (2013).
[32] C. Xu and J. E. Moore, Phys. Rev. B **73**, 045322 (2006).
[33] C. Wu, B. A. Bernevig, and S.-C. Zhang, Phys. Rev. Lett. **96**, 106401 (2006).
[34] T. L. Schmidt, S. Rachel, F. von Oppen, and L. I. Glazman, Phys. Rev. Lett. **108**, 156402 (2012).
[35] J. I. Väyrynen, M. Goldstein, and L. I. Glazman, Phys. Rev. Lett. **110**, 216402 (2013).
[36] J. I. Väyrynen, M. Goldstein, Y. Gefen, and L. I. Glazman, Phys. Rev. B **90**, 115309 (2014).
[37] J. Wang, Y. Meir, and Y. Gefen, Phys. Rev. Lett. **118**, 046801 (2017).
[38] A. Ström, H. Johannesson, and G. I. Japaridze, Phys. Rev. Lett. **104**, 256804 (2010).
[39] F. Crépin, J. C. Budich, F. Dolcini, P. Recher, and B. Trauzettel, Phys. Rev. B **86**, 121106(R) (2012).
[40] J. C. Budich, F. Dolcini, P. Recher, and B. Trauzettel, Phys. Rev. Lett. **108**, 086602 (2012).
[41] C.-H. Hsu, P. Stano, J. Klinovaja, and D. Loss, Phys. Rev. B **96**, 081405(R) (2017).
[42] C.-H. Hsu, P. Stano, J. Klinovaja, and D. Loss, Phys. Rev. B **97**, 125432 (2018).
[43] A. Mani and C. Benjamin, Phys. Rev. Applied **6**, 014003 (2016).
[44] A. A. Bagrov, F. Guinea, and M. I. Katsnelson, arXiv:1805.11700.
[45] J. I. Väyrynen, D. I. Pikulin, and J. Alicea, Phys. Rev. Lett. **121**, 106601 (2018).
[46] P. Novelli, F. Taddei, A. K. Geim, and M. Polini, Phys. Rev. Lett. **122**, 016601 (2019).
[47] M. König *et al.*, Phys. Rev. X **3**, 021003 (2013).
[48] L. Du, I. Knez, G. Sullivan, and R.-R. Du, Phys. Rev. Lett. **114**, 096802 (2015).
[49] C.-Z. Chang, W. Zhao, D. Y. Kim, P. Wei, J. K. Jain, C. Liu, M. H. W. Chan, and J. S. Moodera, Phys. Rev. Lett. **115**, 057206 (2015).
[50] X. Zhang and S.-C. Zhang, Proc. SPIE Int. Soc. Opt. Eng. **8373**, 837309 (2012).
[51] B. Shabbir, M. Nadeem, Z. Dai, M. S. Fuhrer, Q.-K. Xue, X. Wang, and Q. Bao, Appl. Phys. Rev. **5**, 041105 (2018).
[52] Y. Deng, Y. Yu, M. Z. Shi, J. Wang, X. H. Chen, and Y. Zhang, arXiv:1904.11468.
[53] C. Tang, C.-Z. Chang, G. Zhao, Y. Liu, Z. Jiang, C.-X. Liu, M. R. McCartney, D. J. Smith, T. Chen, J. S. Moodera, and J. Shi, Sci. Adv. **3**, e1700307 (2017).
[54] L. Lunczer, P. Leubner, M. Endres, V. L. Müller, C. Brüne, H. Buhmann, and L. W. Molenkamp, Phys. Rev. Lett. **123**, 047701 (2019).

Journal of Applied Physics

Quantum anomalous Hall effect with Landau levels in nonuniformly strained silicene

Cite as: J. Appl. Phys. **126**, 104303 (2019); https://doi.org/10.1063/1.5121189
Submitted: 23 July 2019 . Accepted: 22 August 2019 . Published Online: 11 September 2019

Tian-Bao Lan, Yong Xu, Hui Tan, Jun Wang, and Jun-Feng Liu

Journal of Applied Physics ARTICLE scitation.org/journal/jap

Quantum anomalous Hall effect with Landau levels in nonuniformly strained silicene

Cite as: J. Appl. Phys. **126**, 104303 (2019); doi: 10.1063/1.5121189
Submitted: 23 July 2019 · Accepted: 22 August 2019 ·
Published Online: 11 September 2019

View Online Export Citation CrossMark

Tian-Bao Lan,[1,2,a)] Yong Xu,[2,a)] Hui Tan,[1,2,a)] Jun Wang,[3] and Jun-Feng Liu[1,2,b)]

AFFILIATIONS

[1]School of Physics and Electronic Engineering, Guangzhou University, Guangzhou 510006, China
[2]Department of Physics, Southern University of Science and Technology, Shenzhen 518055, China
[3]Department of Physics, Southeast University, Nanjing 210096, China

[a)]**Contributions:** T.-B. Lan, Y. Xu, and H. Tan contributed equally to this work.
[b)]**Electronic mail:** phjfliu@gzhu.edu.cn

ABSTRACT

We propose a quantum anomalous Hall (QAH) effect with Landau levels in silicene under a nonuniform strain. By applying both a perpendicular electric field and an exchange field, silicene enters a valley-polarized phase first. Then, an arc-shaped strain is used to drive the silicene to a quantum anomalous Hall effect. Landau levels and edge states are numerically obtained in the band structure of a zigzag ribbon. Two-terminal conductance and four-terminal Hall conductance exhibit correspondence plateaus that are robust against nonmagnetic and magnetic impurities. This scheme provides a new platform to search for QAH phases at high temperatures and with multiple edge channels.

I. INTRODUCTION

The underlying mechanisms of the quantum Hall effect (QHE)[1,2] are the formation of quantized Landau levels (LLs). Each LL evolves into gapless chiral edge states at sample edges, which are robust against impurity scattering.[3,4] Therefore, the chiral edge states can act as dissipationless one-dimensional conducting channels and may lead to a new generation of low-power-consumption electronics. However, the realization of the QHE requires a strong magnetic field, which limits real-world applications. In contrast to the QHE under a strong magnetic field, the quantum anomalous Hall effect (QAHE) without an external magnetic field may originate from the interplay between spin-orbit coupling and intrinsic magnetism. Since Haldane's proposal for the QAHE in the honeycomb lattice model,[5] much effort has been devoted to seeking new platforms for realizing the QAHE.[6–12,16–19] Effort has mainly focused on two types of systems: graphenelike honeycomb materials[6–15] and magnetically doped topological insulators.[16–19] Investigations of the second type of system resulted in the first experimental realization of the QAHE in Cr/V-doped (Bi, Sb)$_2$Te$_3$ thin films at a temperature of approximately 30 mK.[20–23] The extremely low temperature greatly hinders real-world applications. Although recent efforts on intrinsic magnetic topological insulators may increase the temperature much,[24] the search for a high-temperature QAHE is still a daunting challenge.

Here, we explore another type of QAHE that also originates from quantized LLs. However, the LLs are not produced by a real magnetic field but by a strain-induced pseudomagnetic field. Theoretical studies[25–28] predicted that an arc-shaped strain can induce a nearly uniform pseudomagnetic field in graphene, and the resultant LLs have been experimentally confirmed.[29–31] The exploration of the strain-induced gauge field has also been extended to other 2D materials, such as two-dimensional crystals of transition-metal dichalcogenides (TMDCs).[32–36] Strain has been proposed to engineer a quantum spin Hall (QSH) insulator in a TMDC such as MoS$_2$.[32] To engineer a quantum anomalous Hall (QAH) insulator, strain must be imposed on a time-reversal breaking phase because the strain itself preserves the time-reversal symmetry. Strain-induced pseudomagnetic fields have opposite signs for charge carriers in the two K and K′ valleys of honeycomb materials. It is reasonable to engineer QAH insulators by imposing a strain on valley-polarized materials or so-called ferrovalley materials.[37] Here, we take silicene as an example to numerically demonstrate that the valley-polarized phases in silicene can be engineered into QAH phases with LLs by strain. Recent studies show that silicene deposited on Al$_2$O$_3$

possesses a close band structure to one of free-standing silicene.[38,39]

We employ the tight-binding approach to simulate an arc-shaped strain in silicene. According to the analysis based on a low-energy effective model, the arc-shaped strain induces a nearly uniform pseudomagnetic field in gapless graphene with linear spectrum.[25–27] In contrast, for gapped silicene with considerable intrinsic spin-orbit coupling (SOC) and under a perpendicular electric field, the pseudomagnetic field is not uniform because of the nonlinear spectrum. Therefore, the tight-binding simulation of the strain effect in silicene with a gap is necessary. Our numerical results show that the arc-shaped strain introduces a nonuniform component of the pseudomagnetic field in the gapped silicene. This nonuniform component makes the LLs become dispersive. Besides, we note that a previous work has studied the manipulation of the QAH phase in graphene by means of the uniaxial strain.[40] This work is quite different in that we provide a new scheme to derive the QAH phase, not manipulate an already existing QAH phase. Finally, it is worthy to note that all our calculations are based on the single-particle picture, and no interactions are considered. However, we argue that the large energy spacings between LLs ensure that the predicted QAH phase should be robust against moderate electron-electron interactions in realistic materials.

The rest of this paper is organized as follows. In Sec. II, we first introduce the tight-binding model to describe the silicene in the presence of a perpendicular electric field, an exchange field, and an arc-shaped strain. Then, we introduce the methods to calculate the band structure of a strained ribbon, two-terminal conductance, and four-terminal Hall conductance. In Sec. III, we present and discuss the numerical results of band structures, two-terminal conductances, and Hall conductances. The impurity effect will also be considered. Finally, the conclusion is given in Sec. IV.

II. MODEL AND METHODS

We consider a silicene sheet in the x-y plane in the presence of a perpendicular electric field E_z, an exchange field M, and a strain. Due to the buckled structure of silicene, E_z generates a staggered sublattice potential of $2\Delta_z$ between A sites and B sites. The tight-binding Hamiltonian of such a deformed silicene with intrinsic SOC is given by

$$H = -\sum_{\langle ij\rangle\alpha} t_{ij} c_{i\alpha}^{\dagger} c_{j\alpha} + \frac{i}{3\sqrt{3}} \sum_{\langle\langle ij\rangle\rangle\alpha\beta} \lambda_{ij} v_{ij} \sigma_{\alpha\beta}^{z} c_{i\alpha}^{\dagger} c_{j\beta} + \Delta_z \sum_{i\alpha} \mu_i c_{i\alpha}^{\dagger} c_{i\alpha} + M \sum_{i\alpha} c_{i\alpha}^{\dagger} \sigma_z c_{i\alpha}, \quad (1)$$

where $c_{i\alpha}^{\dagger}$ and $c_{i\alpha}$ are, respectively, the creation and annihilation operators of an electron on site i with spin α and $\langle ij\rangle/\langle\langle ij\rangle\rangle$ run over all the nearest-/next-nearest-neighbor hopping sites. The first term describes the deformed honeycomb lattice with the modified nearest hopping, t_{ij}. The second term represents the intrinsic SOC with modified strength, λ_{ij}, where $\sigma = (\sigma_x, \sigma_y, \sigma_z)$ is the Pauli matrix of spin and $v_{ij} = +1(-1)$ if the next-nearest-neighbor hopping is anticlockwise (clockwise) with respect to the positive z-axis. The third term represents the staggered sublattice potential,

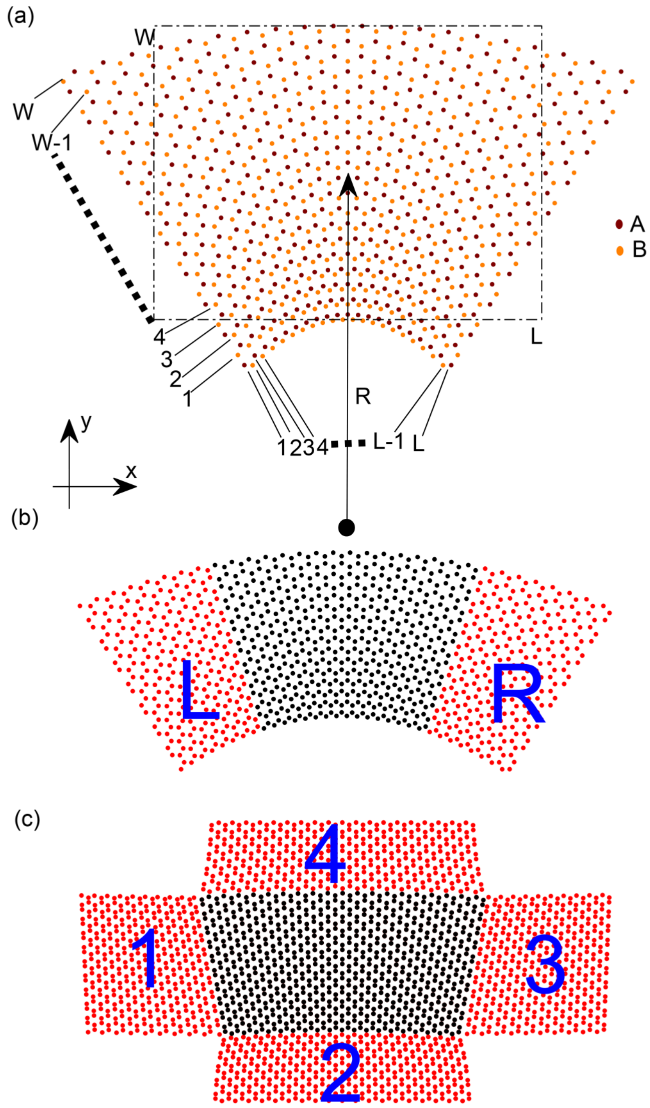

FIG. 1. (a) Sketch of a silicene flake of size $L \times W$ under an arc-shaped strain. (b) The two-terminal device considered for studying the two-terminal conductance. (c) The four-terminal Hall bar considered for studying the Hall conductance.

with $\mu_i = \pm 1$ for the A (B) site. The last term represents the exchange field that may arise due to the proximity coupling to a ferromagnet.[7,41,42]

In the first order approximation,

$$t_{ij} = t\left(1 + \gamma_1 \frac{\delta d_{ij}}{a_0}\right), \quad \lambda_{i,j} = \lambda\left(1 + \gamma_2 \frac{\delta d_{ij}}{\sqrt{3}a_0}\right), \quad (2)$$

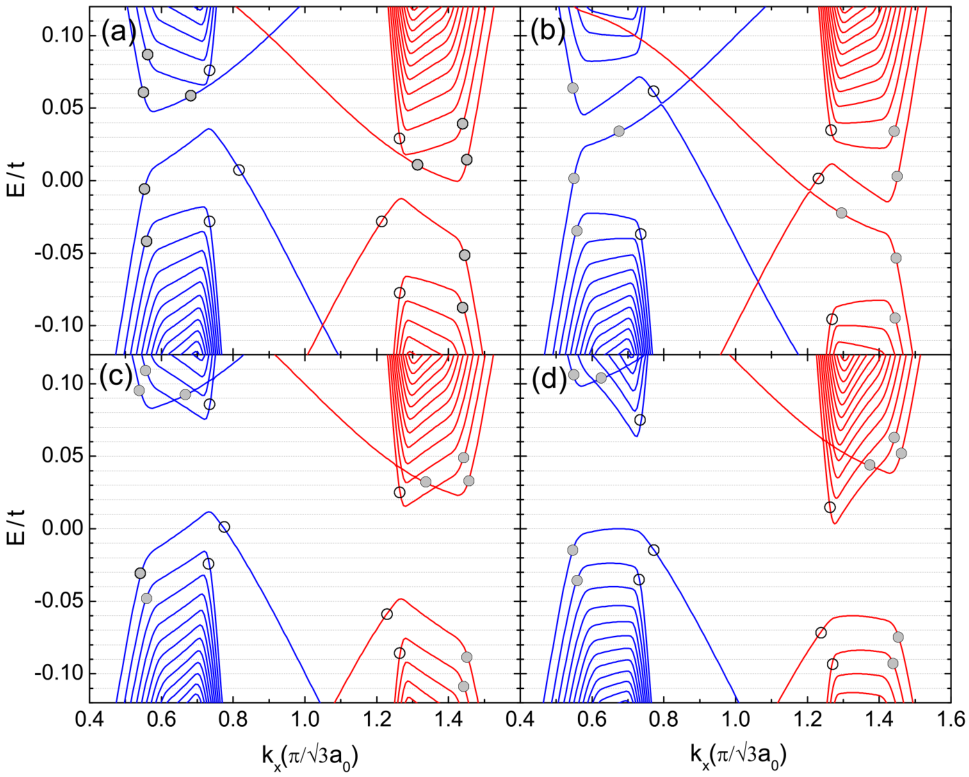

FIG. 2. Band structures of valley-polarized silicene zigzag ribbons under an arc-shaped strain. Blue (red) curves denote spin-up (spin-down) subbands. The solid (hollow) circles denote the top (bottom) edges along which the edge states propagate. (a) $\Delta_z = 0.1$, $M = 0.024$; (b) $\Delta_z = 0.07$, $M = 0.03$; and (c) and (d) $\Delta_z = 0.13$, $M = 0.03$. t is taken as the unit of energy. For (d), a transversal electric field is applied to induce a uniform on-site potential distribution [−0.016,0.016] from the bottom edge to the top edge. Other parameters are $\lambda = 0.1$, the width of the ribbon $W = 500$, and $R = 3W$.

where t and λ are the original nearest hopping and SOC is the strength of unstrained silicene, respectively; a_0 is the Si-Si bond length; and δd_{ij} is the change in the bond length. Here, $\gamma_1 = \frac{d\ln t}{d\ln a}|_{a=a_0}$ and $\gamma_2 = \frac{d\ln \lambda}{d\ln d}|_{d=\sqrt{3}a_0}$. We assume $\gamma_1 = \gamma_2 = \gamma = -2$ in this work. We consider an arc-shaped strain with the in-plane distortions described by[25]

$$(u_x, u_y) = \left(\frac{xy}{R}, -\frac{x^2}{2R}\right), \tag{3}$$

where R is the bending radius, as shown in Fig. 1(a). Such a strain leads to an effective gauge field in the gapless graphene,[43,44] where $\mathbf{A} = (A_x, A_y, 0)$, with

$$\begin{aligned} \mathbf{A} &= \frac{c\gamma}{a_0}(u_{xx} - u_{yy}, -2u_{xy}, 0), \\ u_{\mu\nu} &= \frac{1}{2}\left(\frac{\partial u_\mu}{\partial \nu} + \frac{\partial u_\nu}{\partial \mu}\right), \end{aligned} \tag{4}$$

where μ and ν denote x or y and c is a dimensionless constant. Clearly, the strain described in Eq. (3) leads to a uniform pseudo-magnetic field in gapless graphene or silicene.

From the combination of Eqs. (1) and (3), analytical and numerical investigations show that the arc-shaped deformation approximately preserves the translational symmetry of the system along the x-direction. Therefore, the wave vector k_x approximates a good quantum number. The band structure of such a strained zigzag silicene ribbon with finite width W can be obtained by numerical diagonalization of the Hamiltonian of the ribbon.

Next, we design a two-terminal device shown in Fig. 1(b) to study the longitudinal transport property. The two-terminal conductance from the left lead to the right lead can be calculated using a single-particle Green function,

$$G_{LR}(E) = \frac{e^2}{h} Tr[\Gamma_R G^r \Gamma_L G^a], \tag{5}$$

where $\Gamma_{L(R)}(E) = i[\Sigma^r_{L(R)}(E) - \Sigma^a_{L(R)}(E)]$ and the Green function

$$G^r(E) = [G^a(E)]^\dagger = \frac{1}{E - H_D - \Sigma^r_L(E) - \Sigma^r_R(E)}, \tag{6}$$

with H_D being the Hamiltonian of the device region. The retarded self-energy $\Sigma^r_{L(R)}(E)$ due to the coupling to the leads can be calculated by numerical recursion.

Now, we consider the four-terminal device shown in Fig. 1(c) to calculate the Hall conductance. First, we apply a small bias V between the longitudinal terminals 1 and 3 to study the induced charge current in the transversal terminals 2 and 4. Similar to the two-terminal conductance, the transmission coefficient from terminal q to terminal p can be calculated from the equation $T_{pq}(E) = Tr[\Gamma_p G^r \Gamma_q G^a]$. The current in the terminal p can be

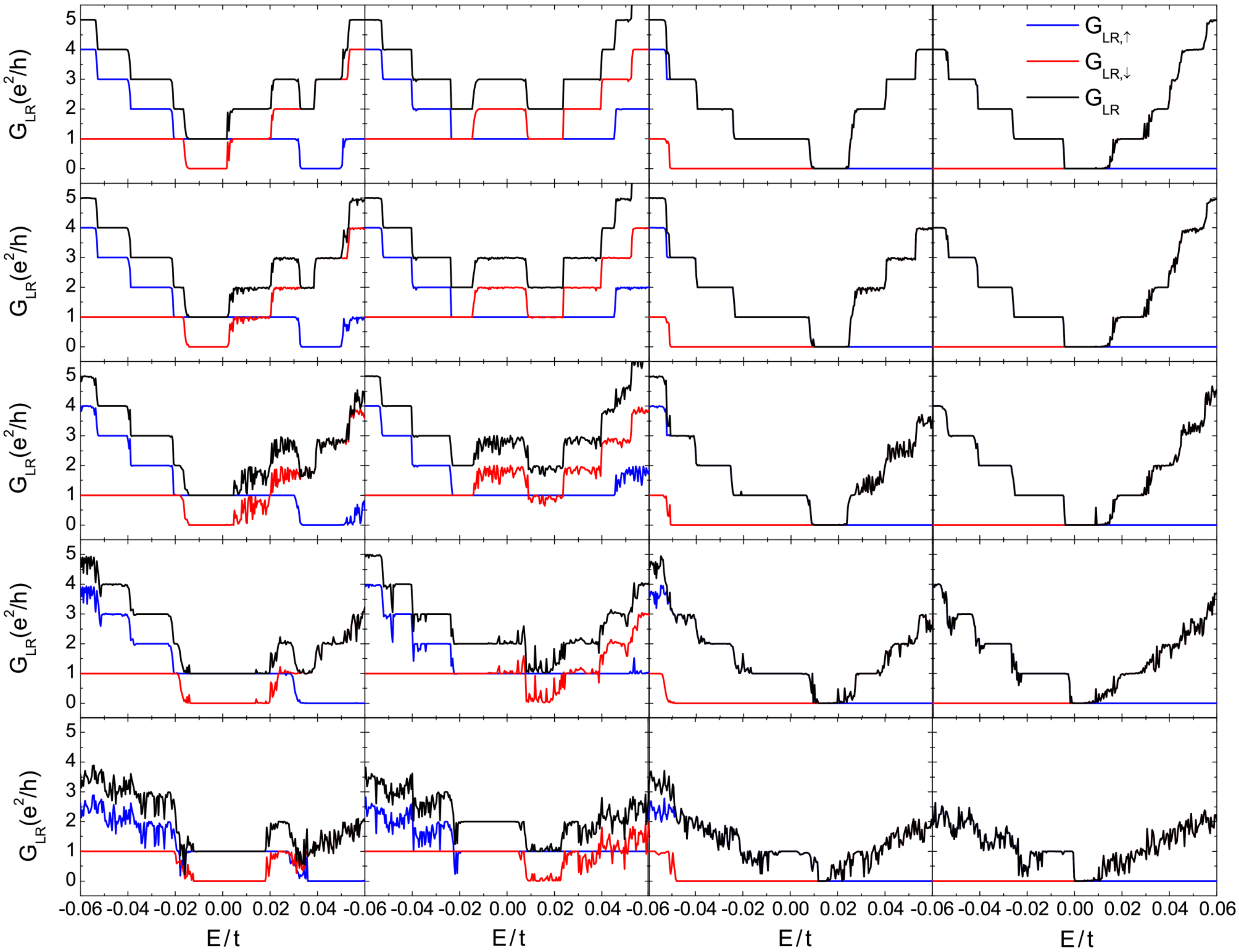

FIG. 3. Two-terminal conductances of the device shown in Fig. 1(b) with various parameters and various nonmagnetic impurity strengths. From left to right, the four columns have the same parameters as those of Figs. 2(a)–2(d). From top to bottom, the five rows correspond to various strengths of nonmagnetic impurity potential, $U_0 = 0$, 0.005, 0.02, 0.1, and 0.3. The length of the scattering region is $L = 1000$.

obtained from the Landauer-Büttiker formula,

$$I_p = \frac{e}{h}\int dE \sum_q T_{pq}(E)[f_q(E) - f_p(E)], \tag{7}$$

where $f_{p/q}(\epsilon) = 1/\left\{1 + \exp[(E - \mu_{p/q})/k_B T]\right\}$ is the Fermi distribution function in terminals p/q, with a chemical potential $\mu_{p/q}$ and a temperature T. In the following numerical calculations, we consider only the zero temperature case ($T = 0$). In the limit of zero bias, the Landauer-Büttiker formula is simplified to $I_p = \frac{e^2}{h}\sum_q T_{pq}[\mu_q - \mu_p]$. Here, the boundary conditions for the four terminals are $\mu_1 = eV/2$, $\mu_3 = -eV/2$, and $\mu_2 = \mu_4 = 0$. The total transversal current flowed across the central scattering area is $I_4 - I_2$. The Hall conductance can be defined as $G_{H,13} = (I_4 - I_2)/V = \frac{e^2}{2h}[(T_{41} - T_{43}) - (T_{21} - T_{23})]$. Similarly, we can apply the bias V between terminals 2 and 4 to calculate the induced charge current in terminals 1 and 3. Then, the boundary conditions for the four terminals are changed to $\mu_2 = eV/2$, $\mu_4 = -eV/2$, and $\mu_1 = \mu_3 = 0$. The Hall conductance can also be defined as $G_{H,24} = (I_1 - I_3)/V = \frac{e^2}{2h}[(T_{12} - T_{14}) - (T_{32} - T_{34})]$. Due to the asymmetric nature of the strained structure, the two Hall conductances generally are not equal to each other. We take the average of these two Hall conductances to determine the real Hall conductance, $G_H = (G_{H,13} + G_{H,24})/2$.

Finally, we also consider the impurity or disorder effect in the calculation of the two-terminal conductance and Hall conductance. The Anderson random impurities are considered in the central scattering region. The nonmagnetic impurities are modeled by the random on-site potential $H_n = \sum_{i,\alpha\beta} U_i c^{\dagger}_{i,\alpha}\sigma^0_{\alpha\beta}c_{i,\beta}$, where σ^0 is the

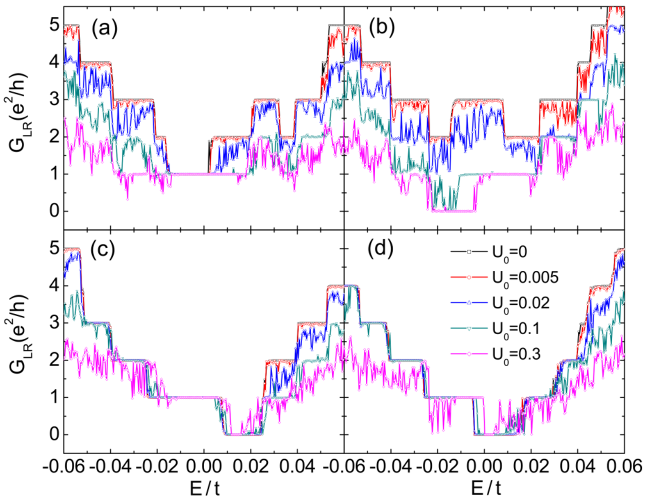

FIG. 4. Two-terminal conductances of the device shown in Fig. 1(b) with various magnetic impurity strengths. (a)–(d) correspond to the phases in Figs. 2(a)–2(d), respectively.

unit matrix in spin space and U_i is the random potential uniformly distributed in the interval $[-U_0/2, U_0/2]$. The magnetic impurities with the magnetization orientation (θ, φ) are modeled by $H_m = \sum_{i,\alpha\beta} U_i(\sigma_z \cos\theta + \sigma_x \sin\theta\cos\varphi + \sigma_y \sin\theta\sin\varphi)_{\alpha\beta} c^\dagger_{i\alpha} c_{i\beta}$. The magnetization orientations are still random and uniformly distributed. Therefore, θ is uniformly distributed in $[0, \pi]$ and φ is uniformly distributed in $[0, 2\pi]$. For all the results presented in this paper, only one impurity configuration is considered, which is sufficient to check the robustness of the conductance plateaus.

III. RESULTS AND DISCUSSION

Figure 2 shows the band structures of three valley-polarized phases under an arc-shaped strain. The three valley-polarized phases are achieved by applying both a perpendicular electric field and an exchange field, which has been suggested in Ref. 45. Without the strain, the effective continuum bulk Hamiltonian around two Dirac cones reads as

$$\mathcal{H}_0 = \hbar v_F(\eta k_x \tau_x + k_y \tau_y) + \Delta\tau_z + \sigma M, \tag{8}$$

where $\tau_{x,y,z}$ are Pauli matrices in the sublattice pseudospin space, $\eta = \pm 1$ for the $\pm K$ valleys, and $\sigma = \pm 1$ for spin-up and spin-down electrons. $\Delta = \Delta_z + \eta\sigma\lambda$ is the gap for electrons with spin σ at valley η. In Fig. 2(b), for $\Delta_z = 0.07$ and $\lambda = 0.1$, Δ changes its sign at the two valleys for both spin-up and spin-down electrons. The sign change of the gap or the so-called band inversion implies that there exist topological edge states crossing the gap and connecting the two valleys, as shown in Fig. 2(b). For Figs. 2(a), 2(c), and 2(d), Δ does not change its sign at the two valleys for a single spin. Therefore, the edge states that connect the two valleys in Figs. 2(a), 2(c), and 2(d) are only the zigzag edge states and do not cross the gap. When the arc-shaped strain is applied, the pseudomagnetic-field-induced LLs are clearly shown. Related to each LL, there are edge states propagating along the edges. Overall, there are three types of edge states in the band structures: zigzag edge states, QSH edge states, and strain-induced edge states. The solid (hollow) circles in Fig. 2 denote the top (bottom) edges along which the edge states are propagating. For the LLs, there are two notable features that are different from the LLs caused by a real uniform magnetic field. One is the absence of the first LL in the conduction bands of (a), (c), and (d) as well as in the valence band of (b). The other is that the LLs become dispersive due to the weak nonuniformity of the pseudomagnetic field. It is shown in (d) that an applied transversal electric field can recover the nearly flat LLs for the valence band at a cost that the LLs in the conduction band become more dispersive.

Figure 3 shows the two-terminal conductances of the device shown in Fig. 1(b) as the same parameters with those in Figs. 2(a)–2(d). Various strength values of the nonmagnetic Anderson random impurities are considered. With only nonmagnetic impurities, the spin-flip scattering is forbidden, and we can present the individual conductance for spin-up and spin-down electrons separately. When $U_0 = 0$, the conductance is well quantized because each conducting channel contributes a conductance quantum. With weak impurities, the conductance plateaus whose energy ranges support both right-going and left-going states with the same spin and at the same edge collapse first. Then, the plateaus related to high LLs collapse when the impurity becomes stronger. The plateaus related to the first LL in the valence band are still robust against strong impurities up to $U_0 = 0.3$. The robustness of the two-terminal conductances against magnetic impurities is shown in Fig. 4. In the presence of magnetic impurities, spin-flip scattering is allowed. In general, the plateaus whose energy ranges host both spin-up and spin-down states are fragile, while those plateaus whose energy ranges host only spin-up or spin-down states have the same robustness as that against nonmagnetic impurities. As shown in Figs. 4(c) and 4(d), the $G_{LR} = 2e^2/h$ plateau in the valence band is robust against magnetic impurities up to $U_0 = 0.1$, which is useful in the development of multichannel topological devices. Additionally, the $G_{LR} = e^2/h$ plateaus remain even for $U_0 = 0.3$ in all four cases.

Next, we examine the Hall conductance by considering the four-terminal Hall bar shown in Fig. 1(c). The spin-up, spin-down, and total Hall conductances in the presence of nonmagnetic impurities are shown in Fig. 5. Figure 6 exhibits the influence of magnetic impurities on the total Hall conductance. Figures 5(a)–5(d) are the Hall conductances for the phase in Fig. 2(a). The $G_H = e^2/h$ Hall plateau is robust against nonmagnetic impurities up to $U_0 = 0.3$ in a wide energy range $[-0.01, 0.012]$. This QAH plateau is a spin-polarized QHE plateau and is also robust against magnetic impurities up to $U_0 = 0.3$, as shown in Fig. 6(a). For the phase in Fig. 2(b), the QSH edge states cross the gap and greatly influence the Hall conductance. There still exist $G_H = e^2/h$ and $G_H = 2e^2/h$ Hall plateaus when the impurity strength is up to $U_0 = 0.1$, whether the impurities are nonmagnetic or magnetic [see Figs. 5(e)–5(h) and 6(b)]. However, there is also a remaining QSH plateau with nonmagnetic impurities of up to $U_0 = 0.3$, which collapses in the presence of magnetic impurities. For the phase in Fig. 2(c), there also exist

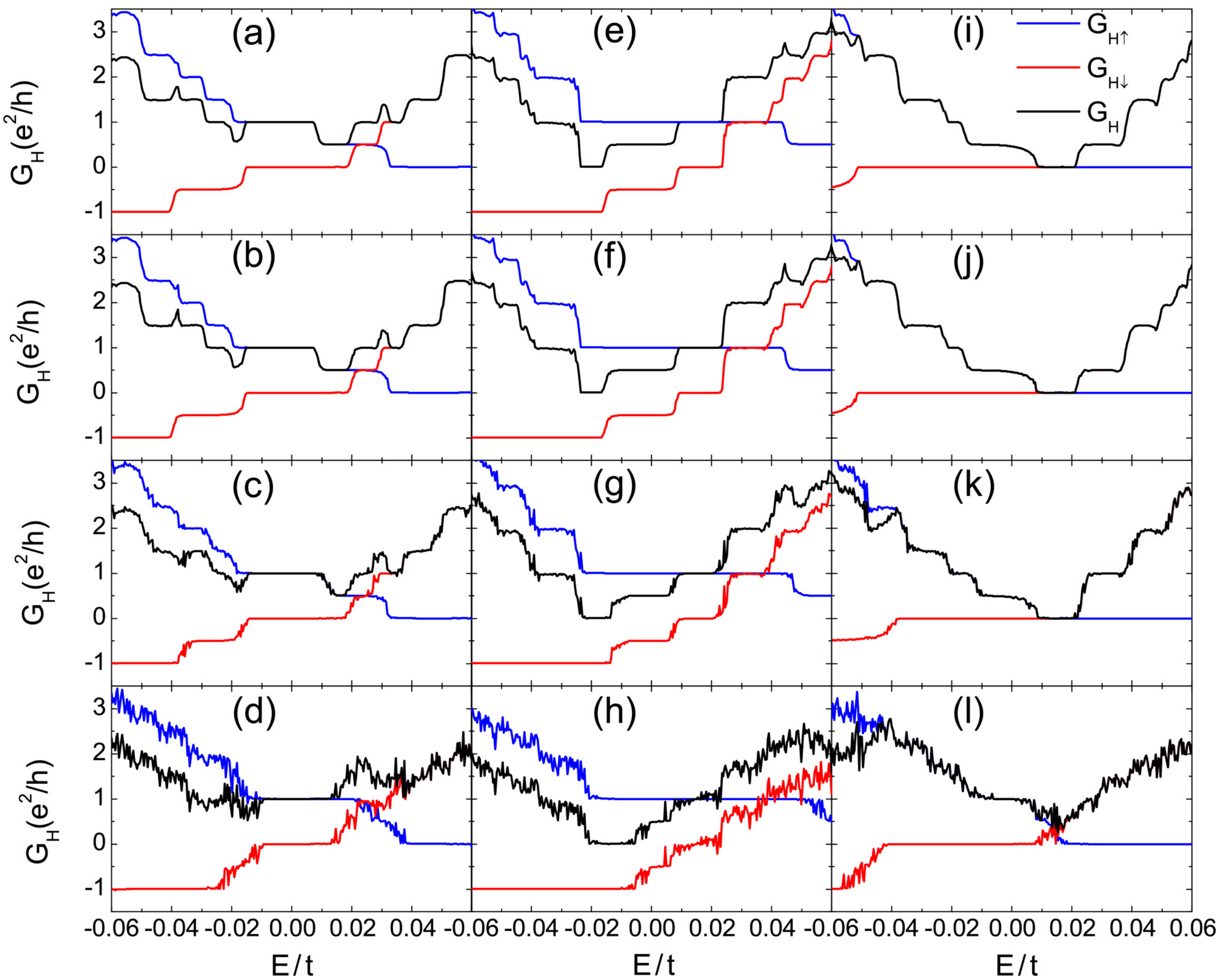

FIG. 5. Hall conductances of the four-terminal Hall bar shown in Fig. 1(c) with various nonmagnetic impurity strengths. From left to right, the three columns correspond to the phases in Figs. 2(a)–2(c). From top to bottom, the four rows correspond to various strengths of nonmagnetic impurity potential $U_0 = 0$, 0.02, 0.1, and 0.3. The size of the scattering region is $W = 500$ and $L = 1000$.

robust Hall plateaus against both nonmagnetic and magnetic impurities up to $U_0 = 0.1$ [see Figs. 5(i)–5(l) and 6(c)]. It is interesting that there is an emergent $G_H = e^2/h$ plateau when the impurity is up to $U_0 = 0.3$ for both nonmagnetic and magnetic impurities.

We give some discussion about near half-integer plateaus in the energy range where the LLs become dispersive. The dispersion of LLs is attributed to the nonuniformity of the strain-induced pseudomagnetic field. In the energy range where the LLs are dispersive, there is only one edge state localized at one edge. Roughly speaking, the dispersive bulk LL has no contribution to the Hall conductance, while the only one edge state contributes $e^2/2h$ to the Hall conductance. From Figs. 5(c), 5(g), and 5(k) and 6(a)–6(c), we see that the $G_H = e^2/2h$ plateau is also robust against both nonmagnetic and magnetic impurities in all three phases until $U_0 = 0.1$. It is noticeable that our numerical results show that the deviation from the half-integer plateaus is only about 10^{-4} e^2/h, while the deviation from some integer plateaus can be less than 10^{-6} e^2/h. This means that the quantization of half-integer plateaus is not as good as that of integer plateaus. We argue that it is because the origin of half-integer plateaus is due to the edge states, but not a bulk Chern number. We argue that the half-integer Hall conductances depend on the four-terminal measurement and do not imply a new topological phase.

Finally, we comment on the experimental feasibility of this proposed QAH phase. By imposing a nonuniform strain on a ferro-valley material, our proposal provides a new scheme to search for

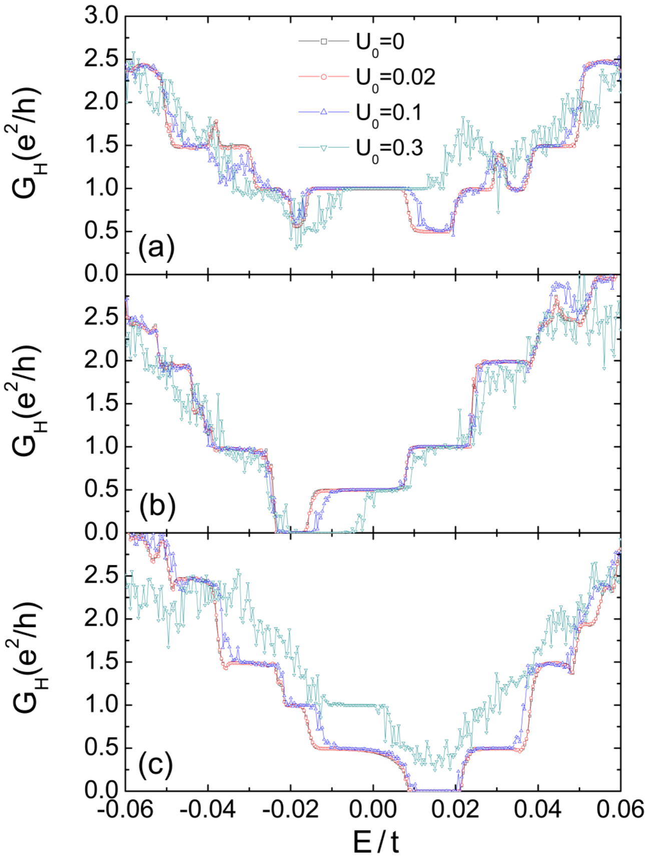

FIG. 6. Hall conductances for various magnetic impurity strengths. (a)–(c) correspond to the phases in Figs. 2(a)–2(c), respectively. The other parameters are the same as those in Fig. 5.

the QAH phase at room temperature. In the example of silicene studied in this work, the largest energy range of the quantized conductance plateau is nearly $0.026t$ [see Fig. 6(a)]. With the hopping energy $t = 1.04\,\mathrm{eV}$ in silicene, the energy spacing $0.026t$ corresponds to a temperature of almost 314 K, which implies the survival of the QAH phase beyond the room temperature. In the present setup, the real challenge for the experimental observation of this proposed QAH phase is how to establish a strong exchange field to get the valley-polarized state.

IV. CONCLUSION

In conclusion, we propose to engineer the QAH phase with LLs in silicene under both a perpendicular electric field and an exchange field under a nonuniform strain. The key idea is to apply the arc-shaped strain to the valley-polarized phases of silicene. Our numerical simulations show well-defined LLs in the band structures. Additionally, the two-terminal conductance and the Hall conductance exhibit robust plateaus against strong nonmagnetic and magnetic impurities as the characteristic transport features of topological edge states. The scheme provides a new platform to search for QAH phases at high temperatures and with multiple edge channels. It is particularly interesting that the half-integer Hall plateaus are also found due to the strain-induced nonuniform pseudomagnetic field and remain robust against nonmagnetic and magnetic impurities.

ACKNOWLEDGMENTS

The work described in this paper was supported by the National Natural Science Foundation of China (NSFC) (Grant Nos. 11774144 and 11574045).

REFERENCES

[1]K. Klitzing, G. Dorda, and M. Pepper, Phys. Rev. Lett. **45**, 494 (1980).
[2]R. B. Laughlin, Phys. Rev. B **23**, 5632 (1981).
[3]B. I. Halperin, Phys. Rev. B **25**, 2185 (1982).
[4]A. H. MacDonald and P. Streda, Phys. Rev. B **29**, 1616 (1984).
[5]F. D. M. Haldane, Phys. Rev. Lett. **61**, 2015 (1988).
[6]M. Onoda and N. Nagaosa, Phys. Rev. Lett. **90**, 206601 (2003).
[7]Z. H. Qiao, S. A. Yang, W. Feng, W.-K. Tse, J. Ding, Y. Yao, J. Wang, and Q. Niu, Phys. Rev. B **82**, 161414(R) (2010).
[8]Z. F. Wang, Z. Liu, and F. Liu, Phys. Rev. Lett. **110**, 196801 (2013).
[9]K. F. Garrity and D. Vanderbilt, Phys. Rev. Lett. **110**, 116802 (2013).
[10]G. F. Zhang, Y. Li, and C. Wu, Phys. Rev. B **90**, 075114 (2014).
[11]J. Hu, Z. Zhu, and R. Wu, Nano Lett. **15**, 2074 (2015).
[12]X.-L. Sheng and B. K. Nikolić, Phys. Rev. B **95**, 201402(R) (2017).
[13]H. Weng, R. Yu, X. Hu, X. Dai, and Z. Fang, Adv. Phys. **64**, 227 (2015).
[14]Y. F. Ren, Z. H. Qiao, and Q. Niu, Rep. Prog. Phys. **79**, 066501 (2016).
[15]C.-X. Liu, S.-C. Zhang, and X.-L. Qi, Annu. Rev. Condens. Matter Phys. **7**, 301 (2016).
[16]C. X. Liu, X. L. Qi, X. Dai, Z. Fang, and S. C. Zhang, Phys. Rev. Lett. **101**, 146802 (2008).
[17]R. Yu, W. Zhang, H. J. Zhang, S. C. Zhang, X. Dai, and Z. Fang, Science **329**, 61 (2010).
[18]J. Wang, B. Lian, H. Zhang, Y. Xu, and S. C. Zhang, Phys. Rev. Lett. **111**, 136801 (2013).
[19]C. Fang, M. J. Gilbert, and B. A. Bernevig, Phys. Rev. Lett. **112**, 046801 (2014).
[20]C. Z. Chang *et al.*, Science **340**, 167 (2013).
[21]J. G. Checkelsky *et al.*, Nat. Phys. **10**, 731 (2014).
[22]X. Kou *et al.*, Phys. Rev. Lett. **113**, 137201 (2014).
[23]C. Z. Chang, W. Zhao, D. Y. Kim, H. Zhang, B. A. Assaf, D. Heiman, S.-C. Zhang, C. Liu, M. H. W. Chan, and J. S. Moodera, Nat. Mater. **14**, 473 (2015).
[24]Y. Gong *et al.*, Chin. Phys. Lett. **36**, 076801 (2019).
[25]F. Guinea, A. K. Geim, M. I. Katsnelson, and K. S. Novoselov, Phys. Rev. B **81**, 035408 (2010).
[26]M. A. Vozmediano, M. Katsnelson, and F. Guinea, Phys. Rep. **496**, 109 (2010).
[27]T. Low and F. Guinea, Nano Lett. **10**, 3551 (2010).
[28]Y. Chang, T. Albash, and S. Haas, Phys. Rev. B **86**, 125402 (2012).
[29]N. Levy, S. A. Burke, K. L. Meaker, M. Panlasigui, A. Zettl, F. Guinea, A. H. C. Neto, and M. F. Crommie, Science **329**, 544 (2010).
[30]J. Lu, A. C. Neto, and K. P. Loh, Nat. Commun. **3**, 823 (2012).
[31]K. K. Gomes, W. K. Warren Mar, F. Guinea, and H. C. Manoharan, Nature **483**, 306 (2012).
[32]M. A. Cazalilla, H. Ochoa, and F. Guinea, Phys. Rev. Lett. **113**, 077201 (2014).
[33]H. Rostami, R. Roldán, E. Cappelluti, R. Asgari, and F. Guinea, Phys. Rev. B **92**, 195402 (2015).
[34]T. Cheiwchanchamnangij, W. R. L. Lambrecht, Y. Song, and H. Dery, Phys. Rev. B **88**, 155404 (2013).

[35]Y. Ma, L. Kou, X. Li, Y. Dai, S. C. Smith, and T. Heine, Phys. Rev. B **92**, 085427 (2015).
[36]A. J. Pearce, E. Mariani, and G. Burkard, Phys. Rev. B **94**, 155416 (2016).
[37]W.-Y. Tong, S.-J. Gong, X. Wan, and C.-G. Duan, Nat. Commun. **7**, 13612 (2016).
[38]L. Tao, E. Cinquanta, D. Chappe, C. Grazianetti, M. Fanciulli, M. Dubey, A. Molle, and D. Akinwande, Nat. Nanotechnol. **10**, 227 (2015).
[39]M. X. Chen, Z. Zhong, and M. Weinert, Phys. Rev. B **94**, 075409 (2016).
[40]G. S. Diniz, M. R. Guassi, and F. Qu, J. Appl. Phys. **114**, 243701 (2013).
[41]W. K. Tse, Z. Qiao, Y. Yao, A. H. MacDonald, and Q. Niu, Phys. Rev. B **83**, 155447 (2011).
[42]Y. Yang, Z. Xu, L. Sheng, B. Wang, D. Y. Xing, and D. N. Sheng, Phys. Rev. Lett. **107**, 066602 (2011).
[43]J. L. Mañes, Phys. Rev. B **76**, 045430 (2007).
[44]F. Guinea, M. I. Katsnelson, and A. K. Geim, Nat. Phys. **6**, 30 (2010).
[45]M. Ezawa, Phys. Rev. Lett. **109**, 055502 (2012).